Numerical Simulation of Surface Effect Ship Air Cushion and Free Surface Interaction

David Johnson Donnelly

Thesis submitted to the faculty of the Virginia Polytechnic Institute and State University in partial fulfillment of the requirements for the degree of

Master of Science
In
Ocean Engineering

Wayne L. Neu
Alan J. Brown
Leigh S. McCue-Weil

September 8, 2010
Blacksburg, VA

Keywords: T-Craft, Surface Effect Ship, Air Cushion, Free Surface, CFD, Volume of Fluid

Numerical Simulation of Surface Effect Ship Air Cushion and Free Surface Interaction

David Johnson Donnelly

Abstract

This thesis presents the results from the computational fluid dynamics simulations of surface effect ship model tests. The model tests being simulated are of a generic T-Craft model running in calm seas through a range of Froude numbers and in two head seas cases with regular waves. Simulations were created using CD-adapco's STAR-CCM+ and feature incompressible water, compressible air, pitch and heave degrees of freedom, and the volume of fluid interface-capturing scheme. The seals are represented with rigid approximations and the air cushion fans are modeled using constant momentum sources. Drag data, cushion pressure data, and free surface elevation contours are presented for the calm seas cases while drag, pressure, heave, and roll data are presented for the head seas cases. The calm seas cases are modeled both with no viscosity and with viscosity and turbulence. All simulations returned rather accurate estimations of the free surface response, ship motions, and body forces. The largest source of error is believed to be due to the rigid seal approximations. While the wake's amplitude is smaller when viscosity is neglected, both viscous and inviscid simulations' estimations of the free surface qualitatively match video footage from the model tests. It was found that shear drag accounts for about a quarter of the total drag in the model test simulations with viscosity, which is a large source of error in inviscid simulations. Adding the shear drag calculated using the ITTC-1957 friction coefficient line to the total drag from the inviscid simulation gives the total drag from the viscous simulations within a 6% difference.

Table of Contents

List of Figures

List of Tables

Nomenclature

R_W	Wavemaking drag due to air cushion
p_c	Air cushion pressure
B_c	Air cushion beam
g	Gravitational acceleration
ρ_w	Water density
C_W	Coefficient of wavemaking drag due to air cushion
U	Characteristic velocity
Δx	Local grid size
Δt	Timestep

Abbreviations

ACV	Air cushion vehicle
CFD	Computational fluid dynamics
CFL	Courant-Friedrichs-Lewy number
DOF	Degree of freedom
LAMP	Large Amplitude Motion Program
LMSR	Large medium speed roll-on roll-off ship
NSWCCD	Naval Surface Warfare Center Carderock Division
RANS	Reynolds-averaged Navier-Stokes
SES	Surface effect ship
SWPE-PD	Sea Wave Pattern Evaluation-Pressure Distributions
VOF	Volume of fluid

1. Introduction

As the capabilities of computational fluid dynamics (CFD) and the availability of computing power grow, CFD is being utilized in an ever increasing number of applications. While CFD has played a role in naval architecture and ship design for some time, a full simulation of both the air cushion and water response under and around a surface effect ship (SES) has not been previously demonstrated. This thesis presents the results of numerical simulations of recent tests of a SES model done at the Naval Surface Warfare Center Carderock Division (NSWCCD). The computations use the commercial CFD code STAR-CCM+ by CD-adapco.

Previous simulations and estimations of SES avoid usingReynolds-averaged Navier-Stokes(RANS) CFD due to the complexity and timeconsuming nature of CFD computations. Doctors and McKesson, 2006, present aprogram they created that models the behavior of SES seals and estimates thedrag components on the SES using simple physics and linearized free-surfacetheory. The linearized free-surface theory is applied to the hull, the aircushion, and the deflected bow seal model. While their method is quickand rather accurate, it has limitations such as not simulating ship dynamicsand assuming a deflected seal shape.

Lin, Zhang, and Weems, 2010, presenttheir SES simulation that uses the Large Amplitude Motion Program (LAMP)with the implementation of several seal and air cushion models to estimatethe SES's motions in waves and create response amplitude operators. LAMPuses a time-domain approach that employs a 3D perturbation velocitypotential and initial value problem to calculate the wave-body interaction,estimate all of the forces and moments acting on the ship, and produce the sixdegrees of freedom (DOF) motions. The air cushion can be modeled bothassuming the air pressure and density inside the cushion is uniform and bysolving the nonlinear Euler equations for compressible flow of an ideal gas.Limitations of this simulation include the accuracy of the seal modeland gaps, the fan characteristics, and the integration of the pressure fromthe air cushion on the interior surfaces.

A program called Sea Wave Pattern Evaluation-Pressure Distributions (SWPE-PD) can be used to determine the shape of the free surface disturbance due to a pressure patch traveling over the free surface at constant speed using velocity potentials and Green's functions, see Scullen and Tuck, 2001. Instead of entering the ship offsets as done in SWPE, in SWPE-PD the pressure distribution is input and treated as a Havelock source in the calculation. Some results of simulations with a constant-pressure patch, a bi-quadratic pressure patch, and tandem pressure patches are presented in Tuck, Scullen, and Lazauskas, 2002. While this program can accurately estimate the elevation of the free surface response to a pressure patch, it cannot do anything else, such as calculate forces like drag, include effects due to side hulls, or allow for any dynamic motions.

The main goal of this work is to explore the possibilities and methods behind simulating a SES usingcommercial CFD software. The simulations are used to explore the complex free surface geometry that develops around and underneath the air cushion and side hulls at various speeds. While the motions and forces on a SES model can be easily determined during model testing, the free surface geometry is difficult to visualize and monitor. Through CFD simulation, this free surface geometry can be measured and easily visualized in many ways. The free surface geometry from the simulated model tests, a comparison of some of the forces and motions of the simulations and model tests, and some further exploration of the capabilities of using CFD to model a SES are presented in this thesis.

1.1 Air Cushion Theory

The concept of the surface effect ship and air cushion vehicle arose from the need for high speed, high payload ships that are not subject to the slamming in seaways of planing craft or the hydrodynamic resistance limitations of displacement ships. The key design feature behind these

concepts is a pressurized air 'cushion' that is trapped between the water and the hull of the lifted body. This decreases contact with the water and free surface, reducing the slamming forces, wavemaking drag, and frictional resistance. A fan replaces the air that escapes the cushion through leakage, keeping the average air cushion pressure constant. The air cushion vehicle (ACV) is completely supported by its air cushion and typically employs a flexible skirt system that encompasses the entirety of the craft and air cushion, allowing it to have little or no draft. The surface effect ship (SES) uses rigid side hulls, similar to a catamaran's, and flexible bow and stern seals to trap the air cushion. The rigid, submerged side hulls cause an increased draft, but their buoyancy and reduction in air leakage allow minimal powering for the lifting air cushion when compared to an ACV. Though the SES and ACV concepts share the air cushion design and their hydrodynamics and motions are similar, they are unique. Only simulations of an SES type design are analyzed in this thesis.

The steady drag components for a SES can be broken into the following components: wavemaking drag due to the air cushionand sidehulls,aerodynamic profile drag, seal drag, friction drag due tothe sidewalls, appendage drag, hydrodynamic momentum drag due to the cooling water for the engines, aerodynamic momentum drag,and drag due to the differential air momentum leakage from the bow and stern seals(Yun and Bliault, 2000). The aerodynamic profile drag, frictional drag, appendage drag, and hydrodynamic momentum drag are similar to those for any other ship. The aerodynamic momentum drag is caused by the air that is pumped into the air cushion that must be accelerated to move with the craft. The drag due to differential air momentum leakage from the bow and stern seal arise from air quickly escaping from the air cushion through the gap betweenthe water surface and seal. This causes a jet effect that pushes on the craft. Increasing the air gap at the stern seal can create a jet thrust behind the craft that will cause a negative drag, or increase the craft speed. The seal drag can be broken down into the seal water friction drag, the seal pressure drag, the seal spray drag, and the seal inertia drag. These encompass all forces on the seals as they deform in waves, drag in the water, or vent.

The wavemaking drag due to the air cushion accounts for a large part of the total drag and can be calculated using Equation 1(Yun and Bliault, 2000), below.

$$R_w = C_w \left[\frac{p_c^2 B_c}{\rho_w g} \right] \tag{1}$$

In this equation R_w is the wavemaking drag, p_c is the cushion pressure, B_c is the beam of the cushion, ρ_w is the water density, g is the gravitational acceleration, and C_w is the wave making drag coefficient which is a function of Froude number and the cushion's length to beam ratio. Equation 1 is valid for a rectangular air cushion with uniform pressure operating in a channel of infinite depth and a width greater than ten times the cushion length.The wavemaking drag due to the air cushion increases with speed until a maximum is reached. At speeds greater than this speed, the drag due to the air cushion decreases, forming a drag "hump" that is due to the wavelengths of waves generated by the pressure cushion and their interaction with the craft. As speed is increased from "pre-hump" speeds to hump speed and higher, the wavelengths grow to significantly longer than the craft, and the wave making drag will decrease. Other factors affecting the air cushion wavemaking drag include the water depth, the acceleration, and the yaw of the air cushion.For an air cushion with a length to beam ratio of four, similar to the SES design discussed in this thesis, the primary drag hump occurs at a Froude number of about 0.8 (Yun and Bliault, 2000, pg. 89).The wave making resistance is proportional to the square of the air cushion pressure and the cushion length to beam ratio. To reduce the effect of hump drag, the length of the cushion can be increased or the beam decreased. Reducing the cushion pressure, which will increase the inner draft, also will decrease the effect of hump drag. While a reduced cushion

pressure can reduce wave making drag, it can significantly add to sidehull drag particularly at higher speeds.

1.2 T-Craft

The Transformable Craft, or T-Craft, is a landing craft prototype being designed to exceed current limitations in speed, range, and load capacity. The Office of Naval Research is funding the design of this concept ship that is capable of transforming into three unique types of ships; a catamaran, a SES, and an ACV. As a catamaran, the T-Craft only uses the buoyancy from its two high length-to-beam ratio hulls, which allow good powering and stability. To transform into a surface effect ship, seals drop between the two hulls creating an air cushionpressurized by fans. With the decreased inner draft and additional lift provided by the air cushion, the wetted surface area is decreased, ideal for high speed powering and motions control. An external skirt drops around the whole ship to transform the T-Craft into an air cushionvehicle. This lifts the rigid hulls completely out of the water allowing beaching and amphibious operations. Some of the main objectives of the T-Craft are the capability to transport ten M1A1 tanks, have an un-refueled range of 600 nautical miles while loaded, a crew size of only two, and the capability to climb a 2% sloping beach(Cooper, 2009). The T-Craft is designed to transit to and from a sea base and is intended to operate in close proximity to a large medium speed roll-on roll-off ship (LMSR) for cargo loading from an external ramp. Figure 1 shows a rendering of a possible T-Craft design by Alion Science and Technology Corp.

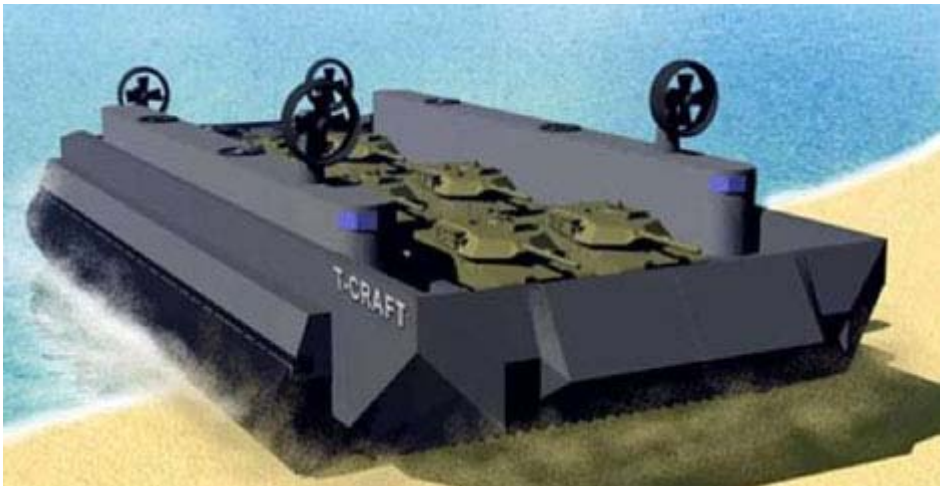

Figure 1: Rendering of beaching T-Craft design by Alion Science and Technology Corp. (Used under fair use)
http://www.marinelog.com/DOCS/NEWSMMVII/2008may00053.html

2. T-Craft Model

The Naval Surface Warfare Center Carderock Division (NSWCCD) completed model testing of a generic T-Craft design operating as a SES both alone and connected to or near an LMSR model in 2008. The generic T-Craft design was designed by John Hoyt, III, and includes design features from each of three contract hull designs from Alion, UmoeMandal, and Textron Marine. The model was built at the NSWCCD model shop, model number 5887. Figure 2 shows the model on cushion in the water. The model features rigid side hulls made of two layers of ¾ inch thick aluminum honey-comb sheeting separated by light density foam board, covered with carbon fiber mats. Three seals separate the air cushion into fore and aft sections. The bow and transverse seals are finger type seals while the aft seal is a double lobe type seal. Figure 3 shows the underside of the T-Craft model, revealing the seal configuration. Two flangemountfour inch blower fans, Jabsco Model 35400-0010, pressurize the air cushions. Channels through the foam board in the hull direct the airflow into the air cushions. Characteristics of the model can be seen in Table 1.

Figure 2: NSWCCD generic T-Craft model (Bishop et al. 2008, used under fair use)

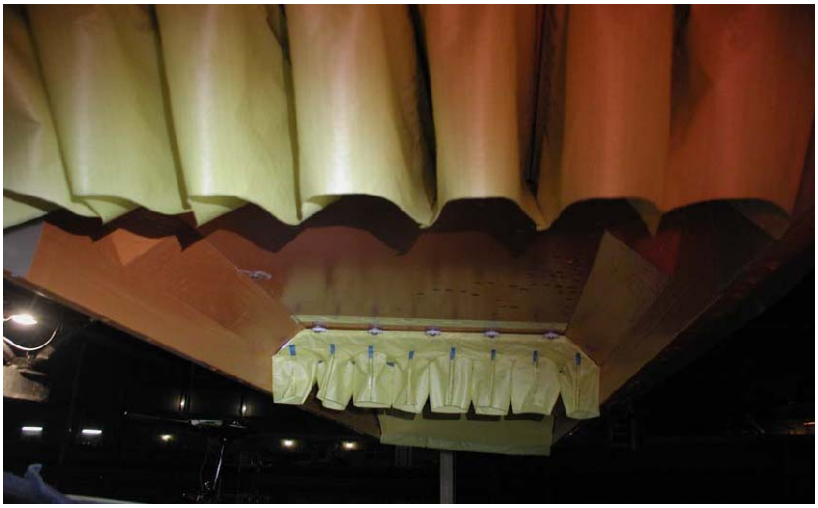

Figure 3: Underside of T-Craft model with seals (Bishop et al. 2008, used under fair use)

T-Craft Model Characteristics	
Linear Scale	1: 30.209
Length Overall	99.5 in, 2.5273 m
Length Waterline (off cushion)	98 in, 2.4892 m
Length Waterline (on cushion)	88 in, 2.352 m
Beam Max	29 in, 0.7366 m
Cushion Width	21.5 in, 0.5461 m
Cushion length	87.5 in, 2.2225 m
Displacement	119 lbs FW, 54 kg – (121.5 lbs from report)
LCG, forward of wet deck transom	48.49 in, 1.231646 m
TCG	0.00 in
VCG, below deck	0.09 in, 0.0023 m (0.25 in from report)
GML	18.6 in
Moment of Inertia in Pitch	20.566 slugs-ft^2
Moment of Inertia in Roll	2.782 slugs-ft^2
Radius of gyration in Pitch	28.44% 2.36 ft
Radius of gyration in Roll	42.25% 0.87 ft
Roll period, model scale from roll decay test	3.66 sec

Table 1: T-Craft Model Characteristics

2.1 ModelTests

The T-Craft model tests mentioned above were conducted during August through October in 2008. The model testing was conducted in NSWCCD's Maneuvering and Seakeeping (MASK) facility allowing testing in calm seas as well asnumerous wave conditions. The MASK facility consists of a 6.1 meter (20 ft) deep basin that is 110 meters (360 ft) long and 73 meters (240 ft) wide, with a 10.7 meter (35 ft) deep trench. It features pneumatic wave makers on two adjacent sides of the basin, each facing 12 degree sloped energy absorbing beaches opposite the basin. The facility's bridge can rotate 45 degrees, allowing any angle heading in waves.

While the test matrix consisted of the T-Craft model and LMSR model in side-by-side, tandem, and Med-Moor conditions, only the tests that involved just the T-Craft are considered for numerical analysis. The model is tested at a variety of speeds, wave conditions, and air cushion pressures. Tests are conducted with full cushion pressure, half cushion pressure, no cushion, or with a Styrofoam insert to represent the air cushion. Table 2 shows the testingconditions of runs that were simulated in this work.

Test Conditions for T-Craft Model Tests			
Run Number	**Froude Number**	**Speed, kts Full Scale**	**Waves**
591	0.08	4	Calm
592	0.2	10	Calm
593	0.4	20	Calm
594, 595	0.6	30	Calm
599	0.6	30	Regular, modal period: 0.787 sec, Wave amplitude: 0.02032 m, 0.8 in
601	0.6	30	Regular, modal period: 0.612 sec, Wave amplitude: 0.0381 m, 1.5 in

Table 2: Test Conditions for T-Craft Model Tests

2.2 Data

To measure and record the relative motions and free surface interactions, several instruments were attached to the model. A Rosemount Vertical Gyro was used to measure T-Craft pitch and roll angles. Three mutually orthogonal BEI Technologies Gyro chip Rate Sensors measured pitch, roll, and yaw rates. Three tri-axial Crossbow solid-state linear accelerometers were attached along the centerline to measure accelerations at the bow, midship, and stern locations of the model. A Qualysis optical motion tracking system used infrared transmitters to measure the relative motions of a passive reflective target located on the T-Craft model. A small load cell that was attached in line with the forward bridal measured the calm water drag. The pressure fans' RPM were measured by an optical transceiver and frequency to voltage converter. When operating with a full cushion the fans ran at 4266 RPM, at 50% cushion the fans ran at 3045 RPM. Four Omega pressure gages, mounted inside the air cushion, measured the model's cushion pressure in the forward cushion, aft cushion, transverse seal, and the stern lobe. Model test data used for comparison to data from simulation has been filtered. Low-pass filtration was gradually increased from 0% to 100% as the frequency increases from 5 to 10 Hz.Further details about the model testing are given in Bishop et al. 2008.

3. Numerical Simulation

The commercial CFD code STAR-CCM+ by CD-adapco was used to create numerical simulations of the model tests. STAR-CCM+ features automated meshing, integrated post-processing, an ever increasing library of solvers and capabilities, and an easy-to-use tree-based user interface. Several of STAR-CCM+'s standard mathematical physics model solvers proved to be valuable to these simulations, which is one of the main reasons the program was used.

The simulations discussed were solved as isothermal and both neglecting viscosity and with viscosity.The governing equations for the inviscid simulations are the Euler equations. These equations are derived by removing the viscosity terms from the Reynolds-averaged Navier-Stokes equations and include a continuity equation and a momentum equation for each of the dimensions. Solving these equations will generate the local pressure and velocity components of the fluid.The viscous simulations discussed have viscosity turned on and use the Spalart-Allmaras turbulence model which solves a single transport equation to determine the turbulent viscosity.STAR-CCM+'s multiphase segregated flow model is used to separate the governing equations for both the water and air. The water is modeled as an incompressible fluid while the air is modeled separately as a compressible ideal gas. This model requires an extra equation, the equation of state, to solve for the compressible air's density.

The Volume of Fluid (VOF) method model in STAR-CCM+ is used to govern the air and water free surface interactions. The volume of fluid method is an interface-capturing type scheme used to capture the free surface between two fluids. Cells are assigned a volume fraction of fluid for each fluid, which sum to one. In this method, the two fluids mix at their interface and the physical properties are taken as averages, weighted by the volume fraction of each of the fluids in these cells. The free surface is considered to be the region between cells comprised entirely of each of the two fluids, or where the volume fraction of either fluid is one half. The convection of the volume fraction requires the solution of an additional transport equation as well as schemes to ensure the region immediately surrounding the free surface remains well resolved (Muzaferija 1998).

The six degree of freedom solver (6-DOF) in STAR-CCM+ allows the computational domain to move in any of the translational or rotational degrees of freedom. When using this model, a solid body is selected that will react to both the natural forces such as buoyancy, drag, and gravity or to user defined forces. Though the reaction to the forces on the body only is computed, the whole computational domain is moved to preserve the mesh. With this model, the domain moves with a body centered local coordinate system while the flow remains moving relative to a global coordinate system. The 6-DOF solver updates the flow field relative to the global coordinates as the domain moves through them. Most of the simulations discussed here have only two degrees of freedom enabled, translational heave and rotational pitch. Some of the simulations have a third degree of freedom enabled in the surge direction.

A VOF waves model is used with the 6-DOF solver to help set up the multiphase domain. The domain is initialized into water and air sections with the free surface level set close to the natural waterline for the stationary T-Craft model, on cushion. The forward velocity is set in this model as the current and wind since the longitudinal degree of freedom is turned off. The free surface can be set up as flat or with either first order or fifth order waves. This model automatically sets up functions to be used for the boundary conditions that will update with the progression of waves.

An additional user-defined field function is used to initialize pressure in the air cushion. Initializing the solution with the free surface close to the natural waterline and with the correct cushion pressure will allow the solution to approach a semi-steady state as quickly as possible, reducing the overall computation time.

The temporal discretization solver is first order implicit unsteady. With this model, solutions are found at time steps and marched through time. For these simulations, twenty inner iterations

between time steps are used to ensure low residuals for higher accuracy. The time step used for each of the simulations is governed by the Courant-Friedrichs-Lewy (CFL) number. The CFL number is the relationship between local grid sizing, Δx, characteristic velocity, U, and the timestep, Δt, and is seen in Equation 2. By limiting the timestep size to give a CFL number of one or less, no more fluid enters a cell than is available in the upwind cell for each timestep. Though simulations using a CFL number greater than one can give solutions, they are not time accurate.

$$\mathrm{CFL} = \frac{U \Delta t}{\Delta x} \tag{2}$$

The simulations discussed use three-dimensional half-models with a symmetry plane down the centerline of the T-Craft model. The computational domain is a rectangular prism that extends three meters in front of, behind, and below the T-Craft; two meters above, and a little more than three meters out from the side of the model geometry. The numerical domain was kept small to reduce the number of cells in the mesh and the total simulation computation time. This may affect the accuracy of the simulation, especially in the far field and near the sides of the domain, however the free surface effects under the air cushion and around the hull are the main focus of these simulations. The forward, bottom, and side (opposite the symmetry plane on centerline) faces are velocity inlets. The aft face is a pressure outlet to allow the disturbed free surface wake to flow through with no reflection of wave energy. The top face is also a pressure outlet to allow air in from the top to be used by the fans, if necessary. The volume fraction, velocity, and pressure settings for these faces are set as pre-determined field functions from the VOF Waves model, discussed more above.Figure 4 shows the domain, bow to the right; orange represents a pressure outlet, red represents a velocity inlet, and blue is the symmetry plane.

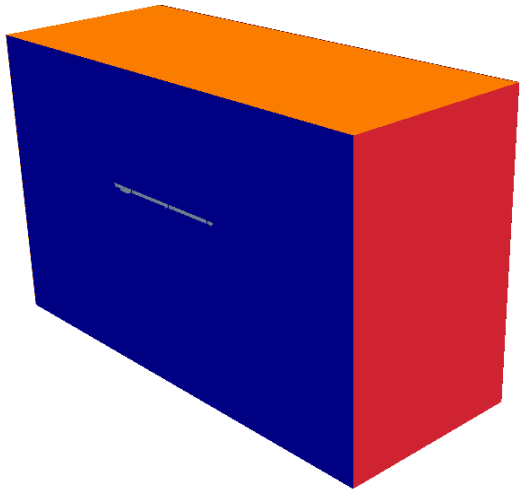

Figure 4: Computational domain; orange is pressure outlets, red is velocity inlets, blue is symmetry plane

4. Preliminary Simulation

The simulations discussed are a culmination of two years worth of CFD and STAR-CCM+ training, research, and simulation trial and error. Several revelations from previous simulation attempts can be seen in the current simulations. Early relevant simulations were very simplified and used as a proof of concept. The first simulation involved a hollowed disk that hovered over a free surface. A central velocity inlet blew air into the hollowed air cushion. The cylinder was a third of the weight of the same volume of water and should sink to a draft that is one third of its height without an air cushion. The necessity to model air as a compressible ideal gas was revealed from this simulation. When air was modeled as incompressible, the pressure in the air cushion would cause large, physically unfeasible gaps in the free surface. Figure 5 shows a disk hovering on the free surface in an early simulation.

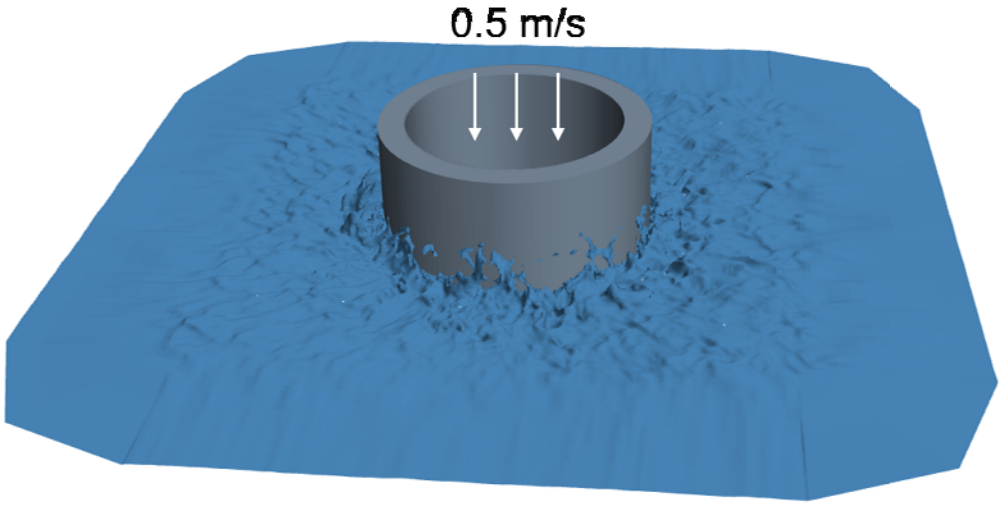

Figure 5: Disk hovering on free surface from early simulations

The next set of simulations used the geometry of the T-Craft model. The T-Craft model's complex rounded finger skirts were modeled as rigid and proved daunting to mesh. As the cells used to capture the complex seal geometry became smaller, the number of cells in the domain grew to unmanageable amounts causing impractical run times. Figure 6 shows the small and irregular surface mesh on the complex bow and stern seal geometries.

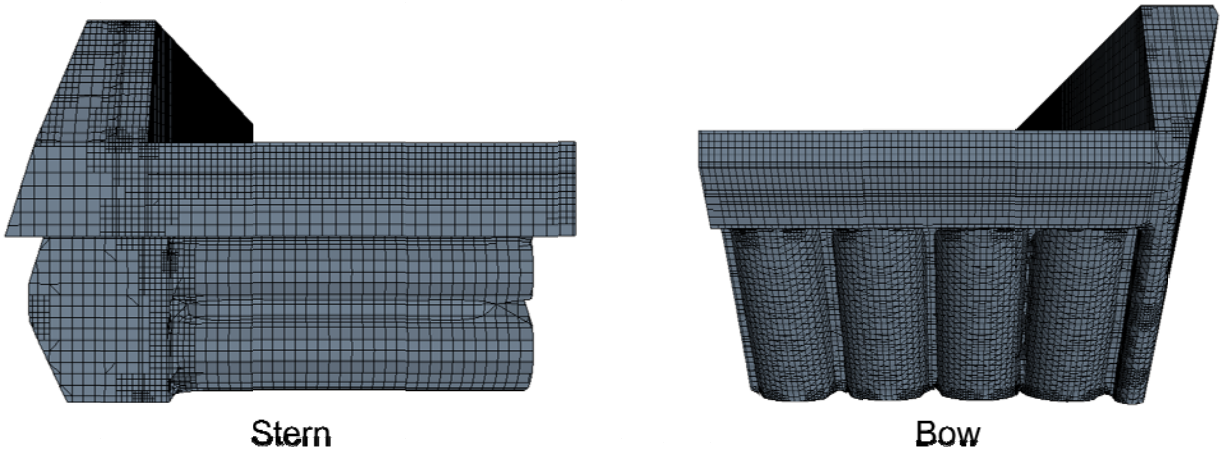

Figure 6: Surface mesh on complex bow and stern seal geometries

From this model, the need for simplified skirts became apparent. This simulation once again used velocity inlets to represent the fans that pressurize the air cushion. Problems using velocity inlets to represent the model's fans also became apparent. The velocity inlets were run at a constant velocity, this represents an infinitely powerful fan whose volume flow does not change with a pressure difference. This constant velocity caused the pressure in the air cushion to rise until the craft completely rose out of the water and released pressure. Also, the velocity inlets would create air and introduce new mass into the computational domainwhich could cause continuity issues, rather than redirecting airflow from the flow field into the air cushion. The fans must be represented by something other than velocity inlets. Figure 7 shows the location of the velocity inlets under the hull. Figure 8 is a view of the free surface from below, it shows that the T-Craft hull is largely out of the water and has an incorrect draft due to the constant air flow of the velocity inlets.

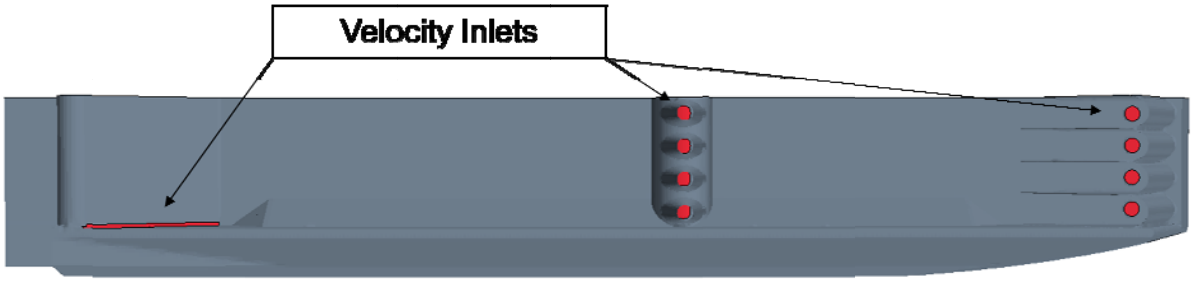

Figure 7: Location of velocity inlets in early simulations

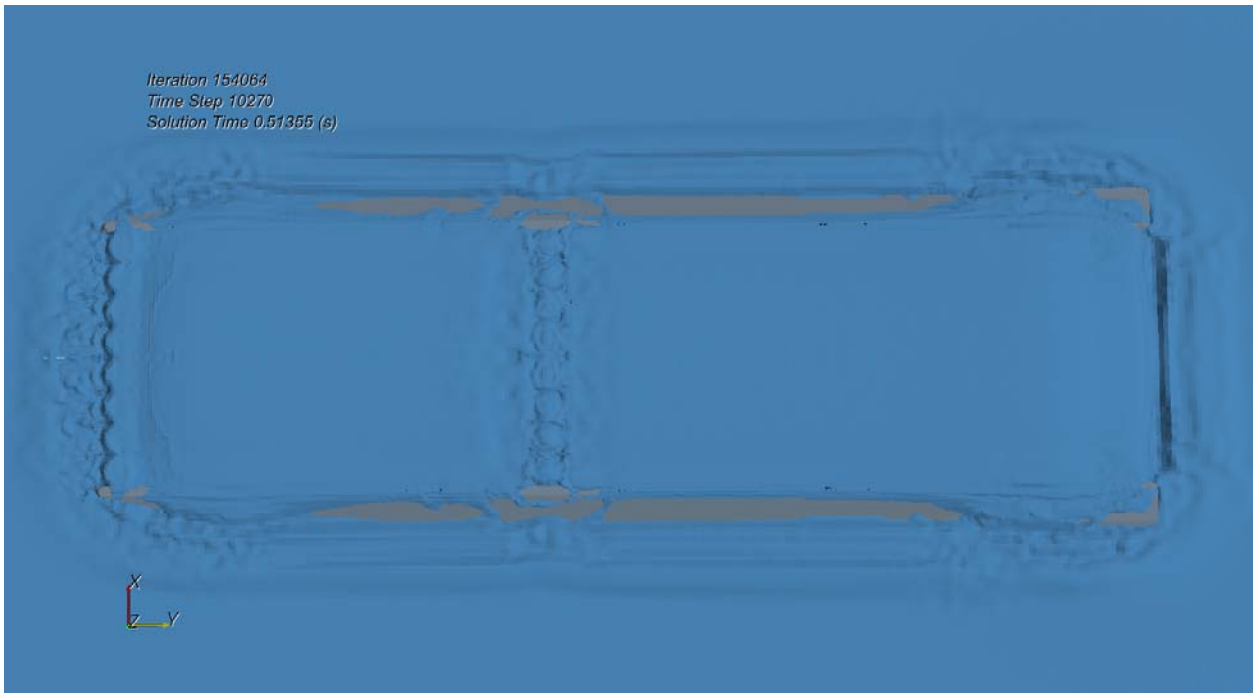

Figure 8: Free surface view from bottom of early simulation, incorrect draft

Once simulations of model testing with forward velocity were attempted, the need for flexible skirts became apparent. The rigid skirts that would extend below the free surface would cause a plowing effect when having a forward velocity. This caused violent heaving and slamming motions as the water would push the skirts up and out of the water. Dynamic and flexible skirts are not yet feasible using Star-CCM+, so to solve the problem, the rigid skirts were shortened to the natural

waterline, leaving an air gap between the skirt and water surface. Figure 9 shows the volume fraction of air of the T-Craft with rigid skirts, plowing through the water. While dynamic and flexible seal modeling is outside the scope of this thesis, the work presented is part of an ongoing study at Virginia Tech that will try to reach this goal.

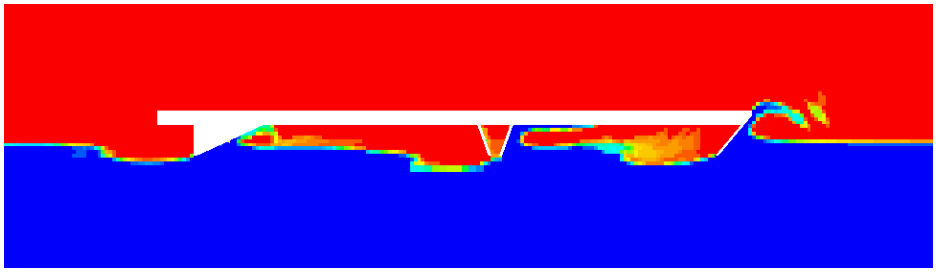

Figure 9: Volume Fraction of Air, T-Craft with rigid skirts plowing through water

5. Recent Simulation

The T-Craft model's seals were simplified for the latest simulations. The bow and transverse finger seals and aft lobed seal are replaced with flat surfaces. This allows larger and more regular surface cells which leads to fewer total cells. Referring to Equation 3, an increased cell size will decrease the CFL number and allow for a larger time step, resulting in a much less computationally expensive simulation. To prevent the plowing effect caused by rigid seals, the seals are shortened to close to the natural waterline. In the model tests, the dynamic seals would inflate with air pressure and fold from water pressure. The rigid seals do not change in the simulation leading to urealistic free surface disturbance and added drag. The simulated rigid seals can be retracted from the water surface completely, thus eliminating all seal drag, but this may alter the pressure distribution on the surface and the craft's response. This condition sets a lower bound on the possible drag value. Once the seals are lengthened to the point where they contact the water surface, the calculated drag will rise quickly with increasing seal length. The goal was to adjust the seal lengths such that a simulation is produced which accurately represents the attitude of the craft and the enclosed pressure distribution without adding the unrealistic effects of dragging rigid seals through the water. The resulting rigid seal length is such that there is only small and intermittent contact with the water surface. This leaves a gap between the seal and the water surface, allowing some air to escape the cushion and water to pass freely or with minimal resistance beneath the seal. For the simulations of the T-Craft model at Froude numbers of 0.2, 0.4, and 0.6, two seal length configurations were used in an attempt to minimize the gap between the free surface and the seals and thus minimize the air leakage. The seal lengths for each configuration were determined through a crude and quick estimation and correction and are cut horizontally. For the Froude number 0.2 simulations, seal configuration "Seals 1" features slightly longer bow and transverse seals than "Seals 2". For the Froude number 0.4 simulations, "Seals 1" has shorter fore and aft seals than "Seals 2" and both seal configurations feature an elongated transverse seal. For the Froude number 0.6 simulations, "Seals 2" features slightly longer bow and transverse seals than the "Seals 1" configuration.All other simulations discussed have the same seal configuration, in which all three seals are shortened to the same length. This is the same configuration as the Froude number of 0.2 configuration "Seals 2" and the Froude number of 0.6 configuration "Seals 1". Figure 10 shows the simplified full draftseals viewed from beneath the model. Figure 11 shows the simplified seals shortened to close to the natural waterline.

Figure 10: Simplified full draftseals

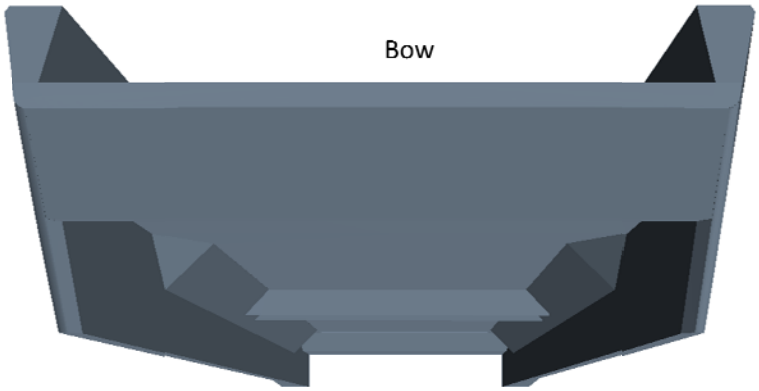

Figure 11: Simplified seals, shortened to close to natural waterline

The fans are represented by volumes known as "momentum sources". These momentum sources add a constant value of momentum through the volume in the desired direction. The momentum added is equal to the pressure on the bottom outlet face divided by the height of the volume or, the force on the bottom face divided by the volume. To reach a desired cushion pressure, the momentum source's momentum value can be changed according to the derivation described above. The momentum source works to keep the cushion pressure fixed by pushing an unlimited amount of air into or out of the cushion as the cushion pressure decreases or increases from the desired value. Using this method to represent the air cushion fans allows outflow through the momentum sources when the cushion pressure exceeds the desired value. A fan curve may be entered into the momentum source to control the amount of airflow through them. Using a fan curve would ensure the correct modeling of the inflow, however it would not ensure accurate cushion pressures since the amount of air leakage out of the cushion is not properly simulated. Because of the uncertainty of the seal modeling, it was found more important to match the cushion pressure rather than the airflow into and out of the cushion. The forward and central momentum sources are located in the same location as the air cushion inlets on the T-Craft model. The aft momentum source is moved slightly forward of the aft lobe seal, since the seal lobes' internal pressures are not simulated. The empty volumes in the hull in Figure 12 are the locations of the three momentum sources.

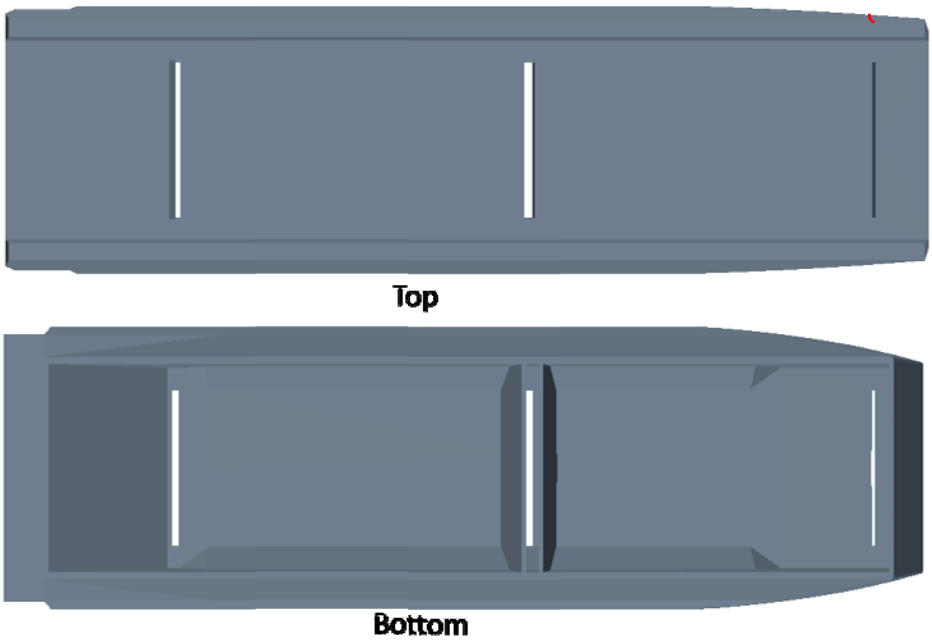

Figure 12: Momentum source locations

The automated meshing and surface mesh editing features in STAR-CCM+ were used to mesh the numerical domain. The mesh model is called a "Trimmer" mesh, which features hexagonal cells. For the inviscid simulations the cell characteristic length on the surface of the craft and in the vicinity of the free surface is two centimeters. Figure 13 shows the surface mesh on the T-Craft model with full seals that have not been shortened for the inviscid simulation mesh configuration. Cell size increases as the distance from the free surface increases with the characteristic length doubling each time the size is increased. This can be seen in Figure 14 which shows the mesh on the symmetry plane. For the inviscid simulations the total number of cells is about 2.5 million. The viscous simulations require a boundary layer mesh, called a prism layer, around the surface meshin order to accurately capture the viscous velocity gradient. For these simulations the cell characteristic length in the vicinity of the free surface is 1.6 centimeters and the surface size is reduced to 0.4 centimeters. The prism layer has five layers that increase in heightfurther away from the surface mesh. Figure 15 shows the prism layer on the symmetry plane at the bow of the T-Craft model. The volume mesh for the viscous simulations is composed of about 3.8 million cells.

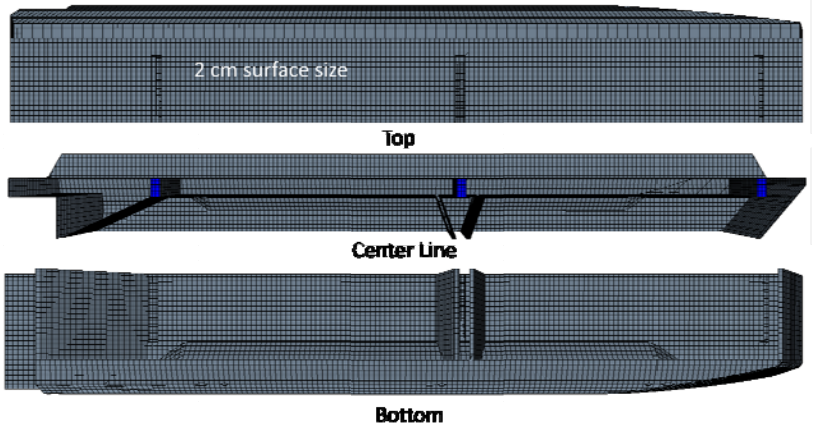

Figure 13: Surface mesh on T-Craft model

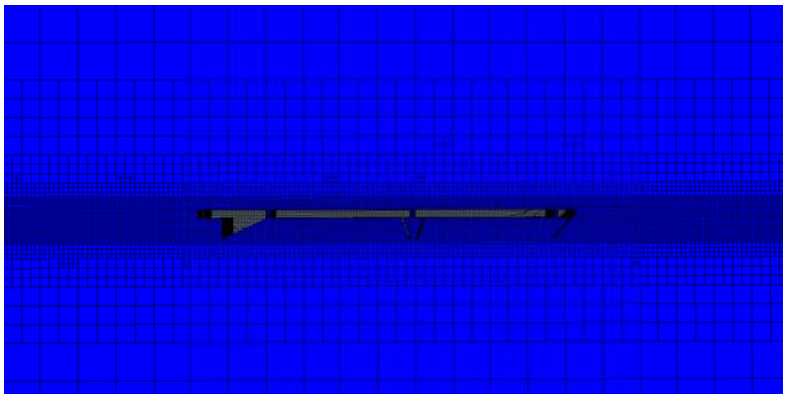

Figure 14: Mesh on symmetry plane

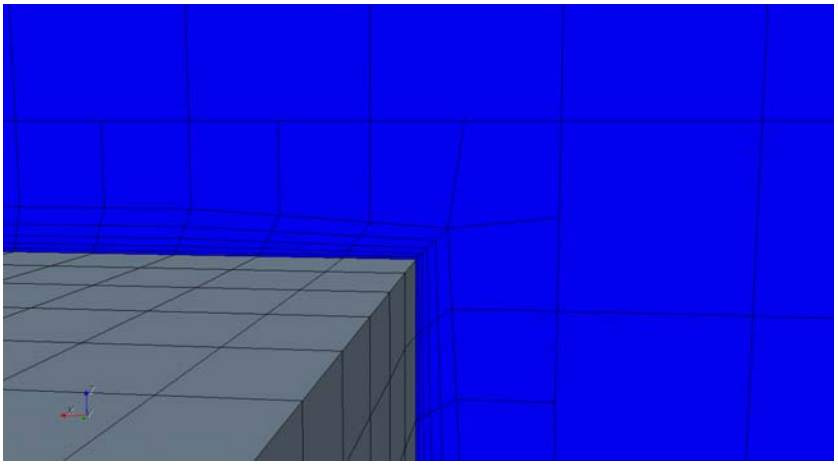

Figure 15: Prism layer mesh on the symmetry plane at aft of T-Craft model

All of the simulations discussed were run using multiple processors on one of three different types of computers. These are the Dell Precision T7400 with two Intel Xenon Quad Core 3.16 GHz processors and 32 GB RAM, the BoxClusterNXi with four Intel Xenon 3.06 Quad Core processors and 48 GB RAM, and Ithaca, Virginia Tech's IBM iDataPlex System on which up to 64 Intel Nehalem 2.26 GHz processors with 24 to 48 GB RAM per node could be used per job.

5.1 Model Test Inviscid Simulation

Though several characteristics of the model testing were monitored, only a few of these characteristics are worth comparing to the numerical simulations. Roll and yaw motions are not used for comparison because they are neglected in the simulations. These motions cannot be simulated using a half model with longitudinal symmetry. Though pitch angle is monitored in both the simulation and the model testing, the zero pitch angle of the model is unknown, preventing comparison. The heave and draft of the simulation is assumed to be correct through matching the cushion pressures, which should result in the correct buoyancy and air cushion forces. Below, comparisons of numerical results with model test data are presented for cushion pressure, drag, and surface elevation contours for calm seas at Froude numbers of 0.08, 0.2, 0.4, and 0.6 which correspond to Runs 591-595 from Table 2.

Simulating the air cushion pressure correctly is vital to the solution accuracy. The air cushion supports much of the weight of the T-Craft while the rest of the weight is supported by the buoyancy force from the side hulls. The cushion pressure dictates the sinkage of the craft and the amount of the craft supported by the side hull buoyancy. At low Froude numbers, the wavemaking drag due to the air cushion makes up a large part of the total drag. For an air cushion with a length to beam ratio close to four, like the T-Craft model, this is true until a drag hump is reached at a Froude number of about 0.8, after which the wavemaking drag due to the air cushion is reduced (Yun and Bliault, 2000). As seen in Equations 1 and 2, the total wavemaking drag due to the air cushion is sensitive to changes in pressure as the pressure term in the equation is squared. For these simulations, air cushion pressure is monitored at the same locations it was measured during the model tests except in the stern lobe seal, since the lobe pressure was not modeled. These locations are in the forward cushion, the transverse seal, and the aft cushion. Figure 16 shows a plot of the simulation's air cushion pressure monitors compared to those from the model test for a Froude number of 0.6. Cushion pressure results for all of the simulations of the calm seas model testing are similar to those presented in Figure 16.

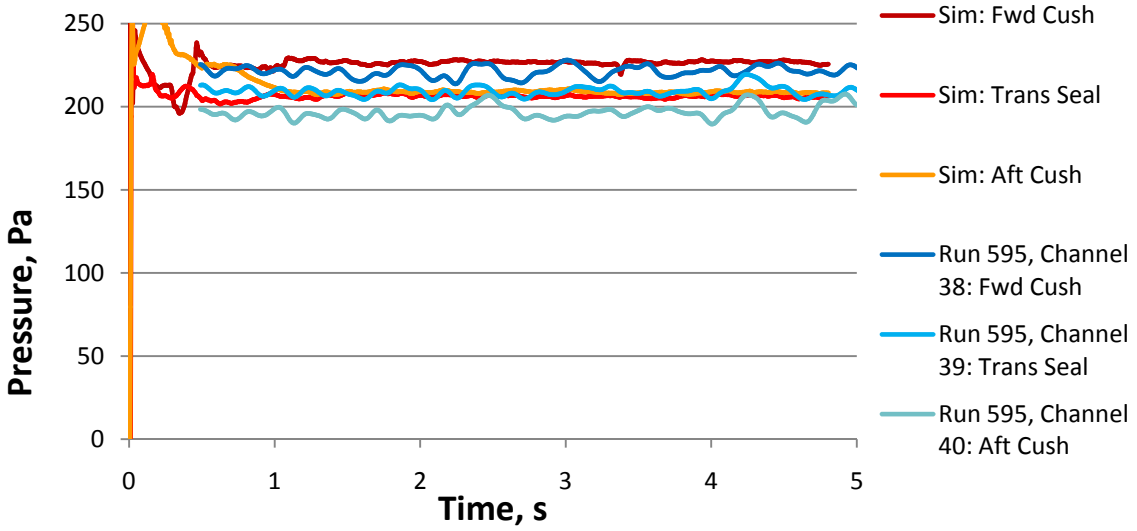

Figure 16: Air cushion pressure monitors, Fn=0.6

It can be seen that the air cushion pressures are very close when comparing the simulation to the model test. The average forward cushion pressure is only about 2.5% off, the average transverse seal pressure is less than 0.2% off, and the aft cushion pressure is about 4% off. The pressure is not constant but fluctuates around a mean value. The simulation's cushion pressure does not fluctuate as much as the model test's due to the constant momentum fan approximation and rigid seals . While the momentum source strength is calculated using the difference between pressures on the outlet and inlet face of the momentum source, as described above, some adjustment was done on each run to get the average pressure values to within about five percent of the values from the model tests. These adjustments were necessary since the pressure on the inlet face of each momentum source was not always zero and the pressure sensors' locations are not on the outlet faces of the momentum sources.Large differences in forward and aft cushion pressures proved difficult to simulate due to the shortened, rigid, transverse seal that depending on the gap distance from the free surface, may not completely separate the air cushion into forward and aft sections.

As discussed earlier, SES total drag is the sum of several factors. Some components of the drag are not correctly simulated or calculated at all in the simulations being discussed. Skin friction on the hull and seals is not modeled at all since the air and water are treated as inviscid. Simulating the seals as rigid may be another source of error. As mentioned above, the goal was to adjust the seal lengths such that a simulation is produced which accurately represents the attitude of the craft and the enclosed pressure distribution without adding the unrealistic effects of dragging rigid seals through the water. The resulting rigid seal length is such that a small gap between the free surface and the seal is left, allowing water to pass under the seal freely and air to escape the cushion. The fact that the resulting total drag calculated is close to the measured drag is one indication of the accuracy of the drag from the air cushion and inviscid side hull effects. While seal length could be adjusted to match the measured drag, this is artificial manipulation of the simulation and was not attempted. Drag data for a Froude number of 0.6 is compared in Figure 17. In this figure, drag from simulations of two different seal length configurations are presented. Drag results for all of the simulations of the calm seas model testing are similar to those presented in Figure 17.

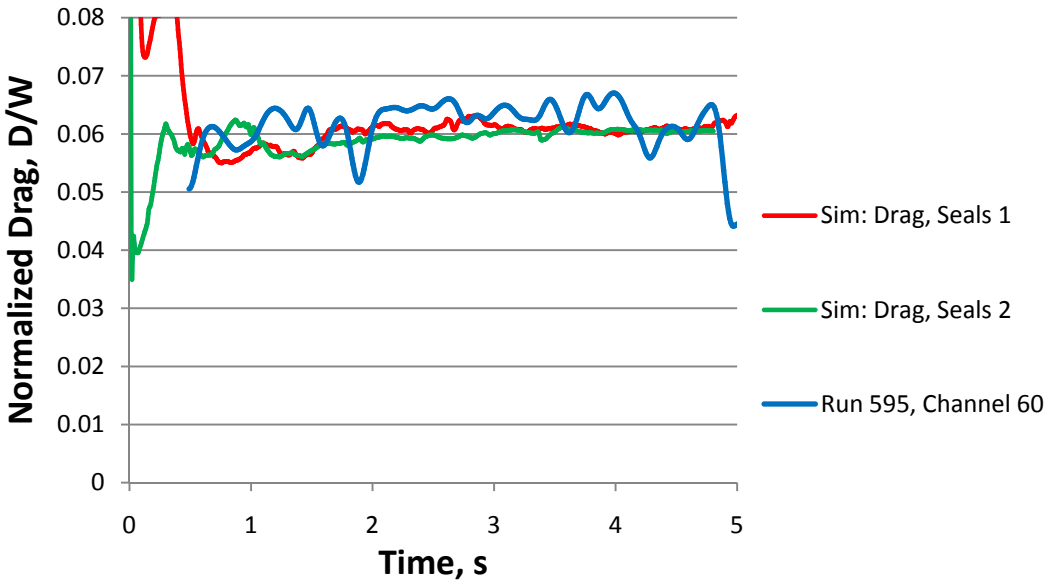

Figure 17: Normalized drag for simulations and model test, Fn=0.6

The simulations' and the model test's drag values are very close. The average drag for the simulation with seals configuration "Seals 1" is about 4.5% off and about 6.5% off for seals configuration "Seals 2". It can be seen that during model testing, the drag fluctuates more than in the simulations. Drag values from the simulations before one second diverge due to the initialization of the flow field. It takes a second or two of simulation time for the flow field to react to the boundary conditions and become steady. Figure 18 shows average drag data from each of the simulations and model tests. The two data series labeled "Run Statistics" and "Report" are both from model testing, however the data labeled "Report" has a correction factor added to it (Silver, 2010). For each of the simulations, drag data is averaged starting after two seconds of run time to allow the flow to develop from initial conditions and become steady. It can be seen that the average drag values between simulations and model testing are comparable. The average drag data for the simulation of a Froude number of 0.2 shows the most error, about 50%. For a Froude number of 0.2 and 0.6 changing the seal length slightly did not have much effect on the drag, however at a Froude number of 0.4 it did. For the simulations with a Froude number of 0.4, the fore and aft seals were lengthened slightly for the second seal configuration. This caused the rigid seals to penetrate the free surface which causes an increase in drag as the rigid seals plow through the water.

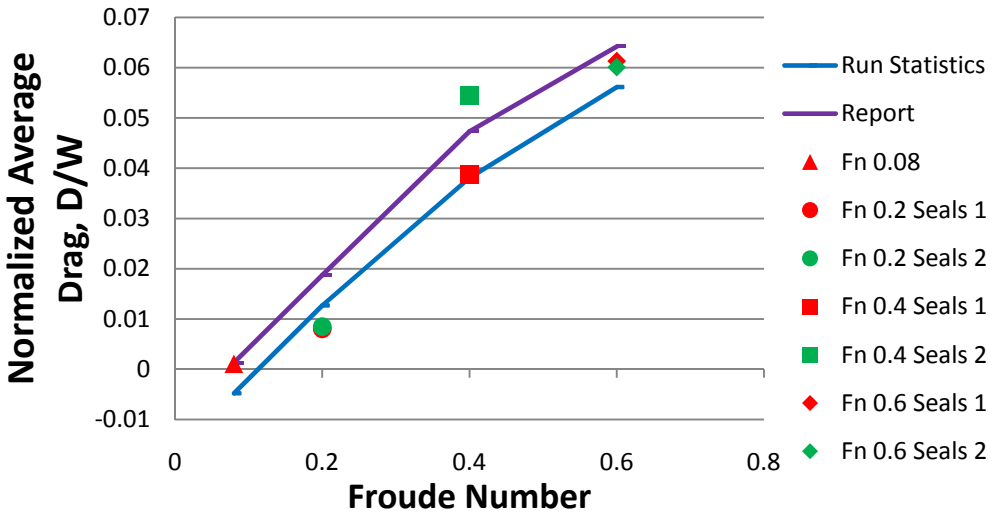

Figure 18: Normalized average drag for simulations and model tests

Examining the free surface around and especially beneath the hull and air cushion can prove to be very valuable in design. Flow features can be observed that may lead to changes in the design of the cushion seals or hull form. Figure 19 shows the simulated free surface elevation contours from each Froude number tested, presented on the same scale for comparison. In the figure, the hull is made transparent and the white areas show where the side hulls pierce the free surface. Though throughout the simulations these contours had small variations over time, the main flow features are present for the simulations' entirety. Small changes in the seal length did not prove to have a considerable effect on the free surface patterns.

After examining the free surface elevation contours it is clear why the air cushion is the cause for a lot of the wave making drag at low Froude numbers. Internal waves under the cushion and between the hulls can be seen at each of the Froude numbers. At the lowest velocity, Froude number of 0.08, there are many waves between the hulls that have a short wavelength. As the craft accelerates to a Froude number of 0.2, the wavelengths grow to about a quarter of the T-Craft's length with four full wavelengths visible between the hulls. At a Froude number of 0.4 the wavelength grows to almost the entire length of the T-Craft. Notice how the second wave hump is located towards the stern of the craft and clearly interacts with the aft seal. The wavelength grows to longer than the ship at a Froude number of 0.6 and the wave trough is close to the stern of the T-Craft. It can be seen that though the wave patterns at lower Froude numbers are much more complex, the amplitude of the waves is much smaller. It is important to note that these internal waves are not two dimensional but rather vary across the beam of the ship as well. This three-dimensionality may be due to the wavemaking of the side hulls and the waves' interactions between them. Note the angle of the crest relative to the hull in the surface elevation contours from the Froude number 0.4 simulation.

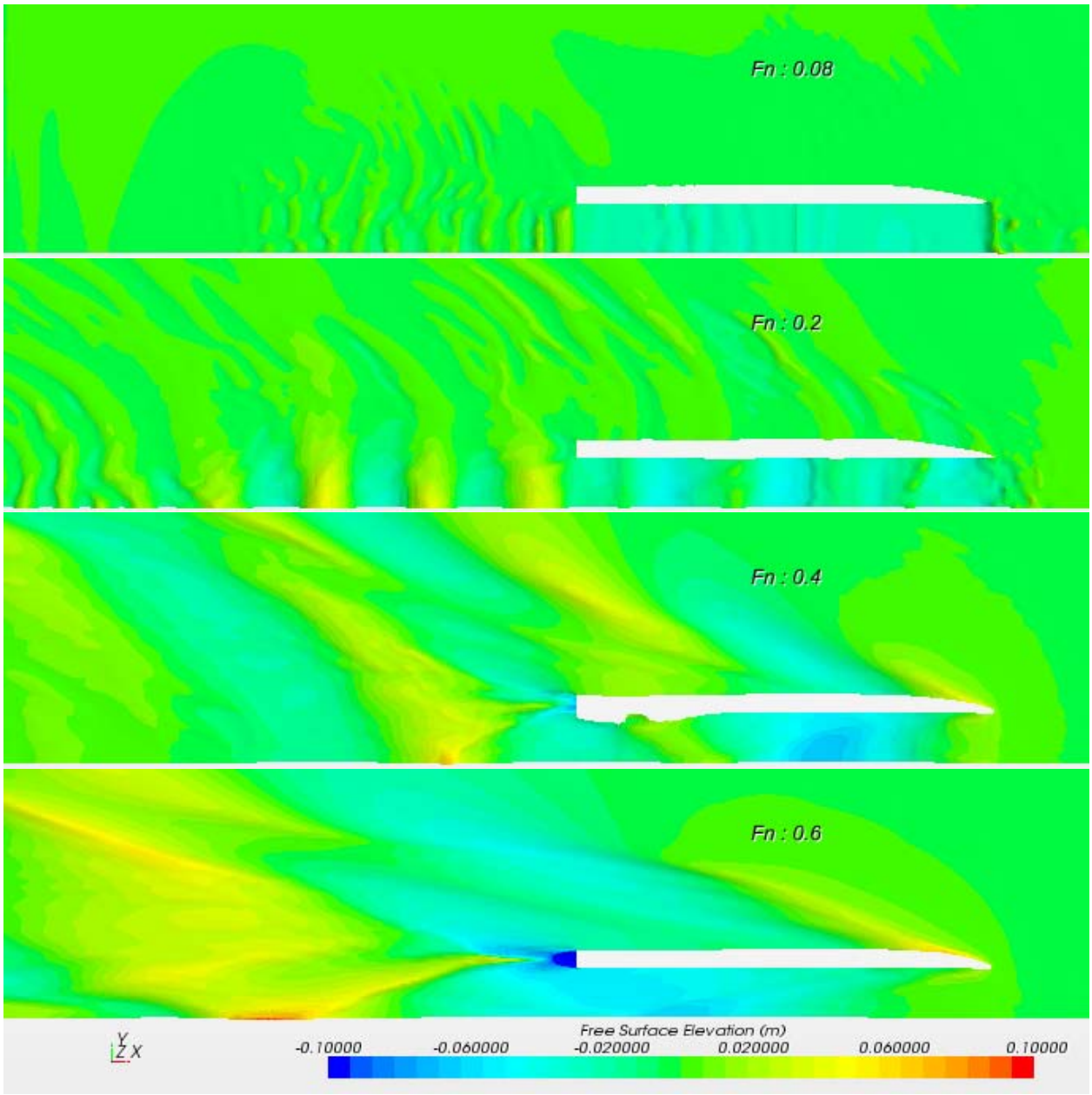

Figure 19: Free surface elevation contours plotted with same scale

Simulations of the two regular wave cases at a Froude number of 0.6, corresponding to Runs 599, and 601 from Table 2, were also conducted; data from both of these cases is presented. It is important to note that while the wave height and frequency of the waves are accurate in the simulation, the phase in time is not. For the plots presented, the time values have been shifted to match the wave phase. For Run 599 the time shift was done by using the heave data as a phase reference. An error with the optical motion tracking systemin Run 601 prevented heave and pitch data from being recorded, so the pressure data is used to shift the time values. Since the incident wave frequency is matched between the model test and the simulation, the predominant frequencies of the responses agree. The average values of the heave and pitch data for the simulation and model test are set to zero, to make comparing oscillation amplitudes easier.

Figures20 and 21show the pressure in the forward cushion for the regular waves simulations and model tests, at the same location as in Figure 16. Like the calm seas runs, the average air cushion pressure between the model tests and simulations are close, within 7% for Run 599 and 11% for Run 601, however, the simulations' pressure fluctuations are more complex than those from model testing.The data collected during model testing was run through a low-pass filter, with filtration gradually increasing from 0 to 100% as frequency increases from 5 to 10 Hz, before being presented here. Figure 22 shows the forward cushion pressure data collected from the model test Run 599 both filtered and unfiltered. The spikes seen at the beginning of the drag peaks for the simulation can also be seen in the unfiltered data. The simulation of Run 599 accuratelyestimates the maximum cushion pressure found in the model test but does not show as large of a pressure drop.This may be attributed to the approximationof the fans as momentum sources that will pressurize the air cushion much quicker than blower fans. Data from both the model test Run 601 and its simulation show two humps at the peak and trough of the pressure fluctuations, however in the simulation they are more pronounced. Both the maximum and minimum values of the pressure are overestimated in the simulation, indicating the momentum source's strength may need to be lowered slightly.

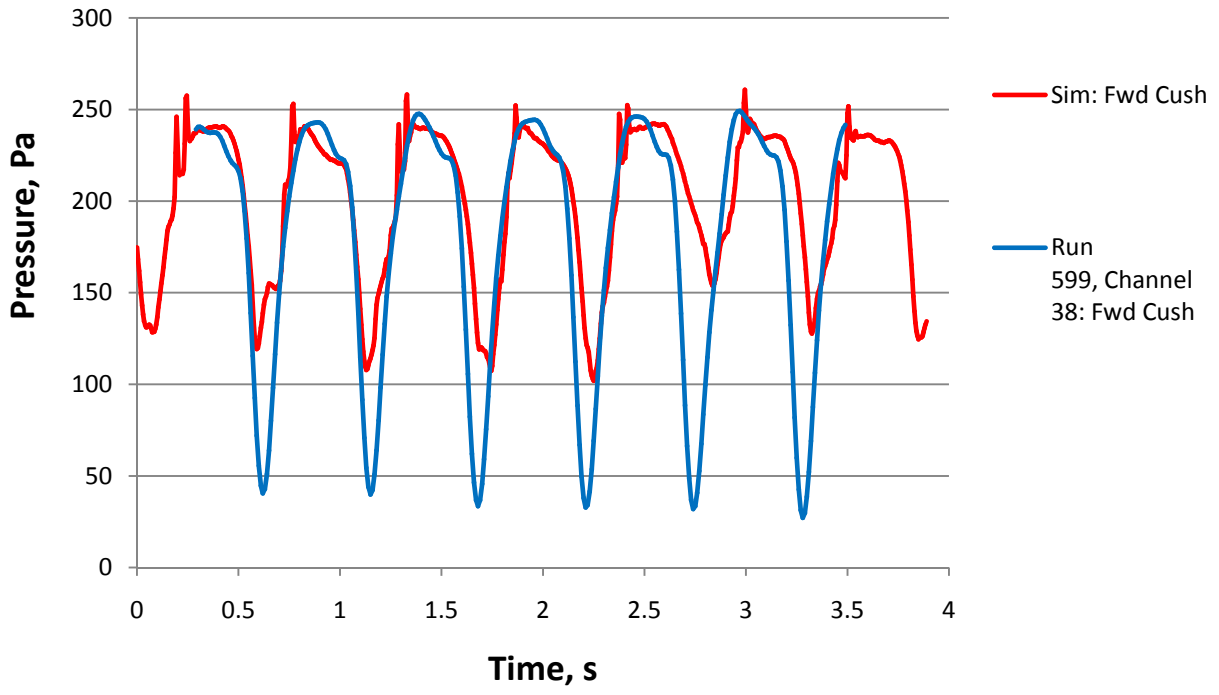

Figure 20: Forward air cushion pressure comparison, Run 599

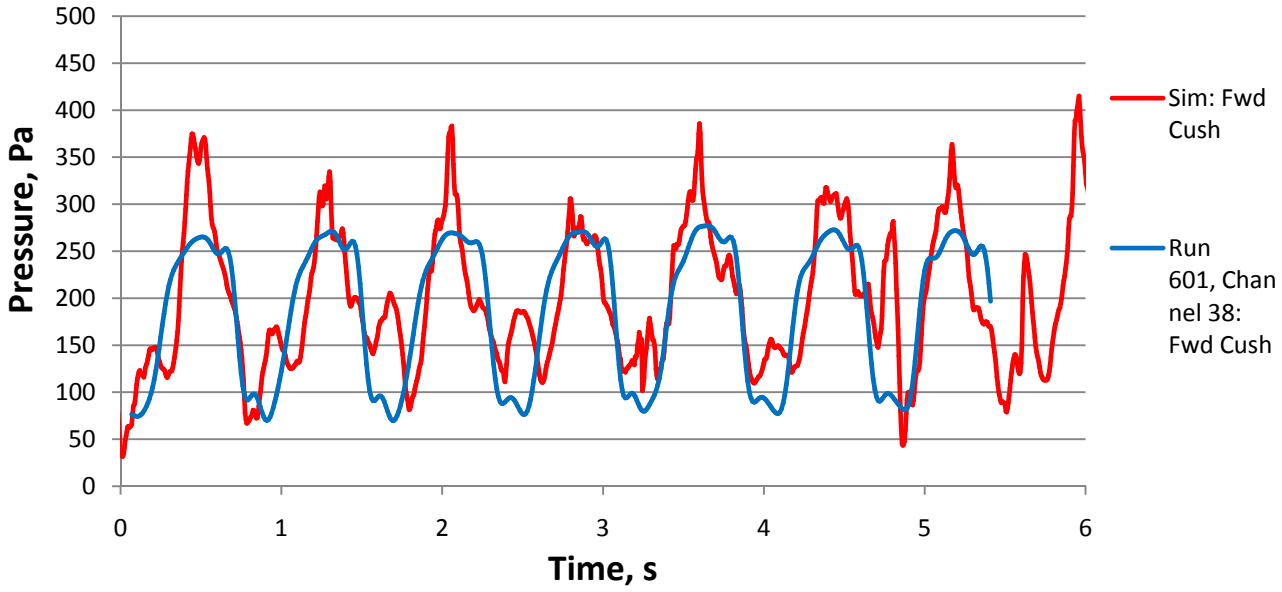

Figure 21: Forward air cushion pressure comparison, Run 601

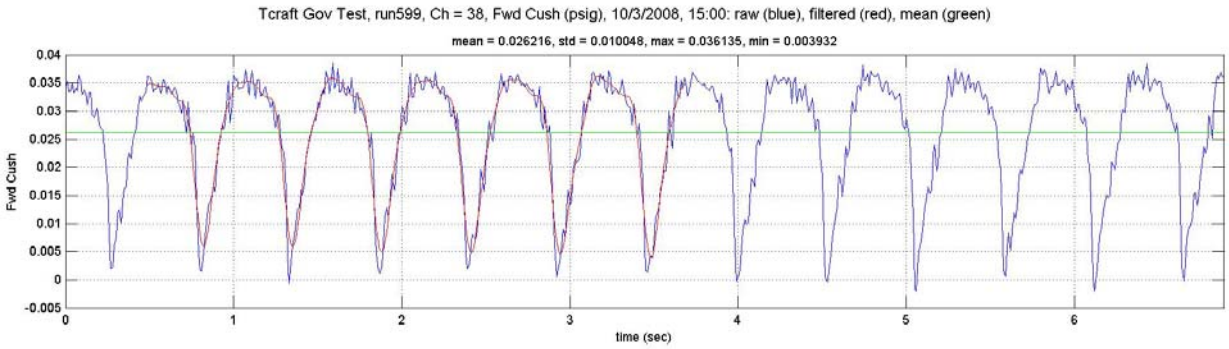

Figure 22: Unfiltered and filtered forward air cushion pressure data, model test Run 599

Figures23and 24show the heave and pitch motions for model test Run 599 and its simulation. In the simulation the heave and pitch is measured from the model's center of gravity while in the model test they are measured about eight inches aft of that. The heave data from the simulation has almost twice the amplitude and much more regular fluctuations than the model test. Adjusting the heave fluctuations from the point where it was measured in the simulation to where it was measured in the model test reduces this error, but does not account for all of it. The simulation's adjusted heave values are also plotted in Figure 23. Another source of error may be due to the cell size in the vicinity of the craft which is larger than the heave motions found in the model test, giving too poor of a mesh resolution to accurately capture the small heave motions in the simulation. The simulation accurately estimates the pitch of the craft, though the amplitude of the fluctuation varies slightly more in the simulation.

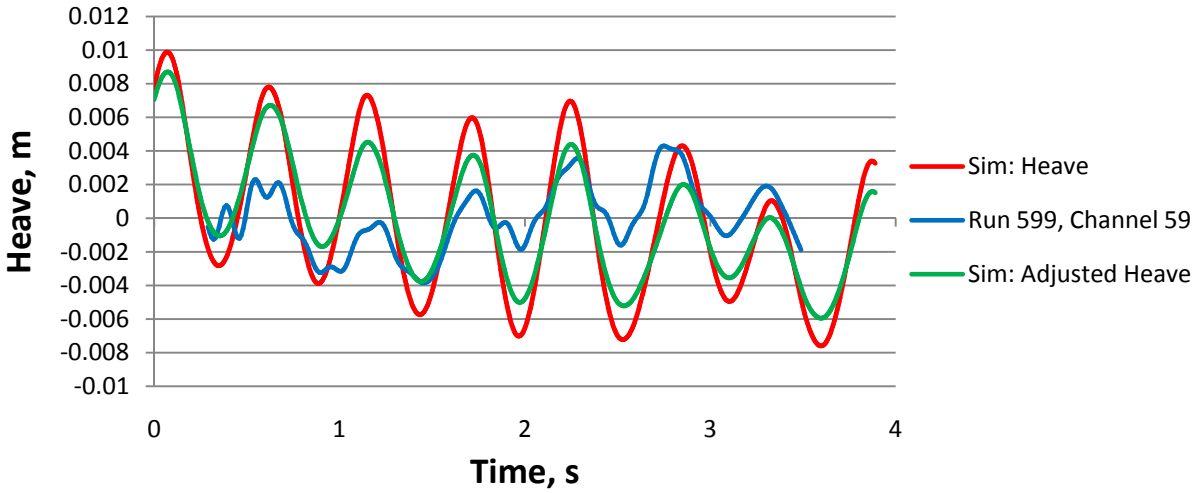

Figure 23: Heave motion amplitude comparison, Run 599

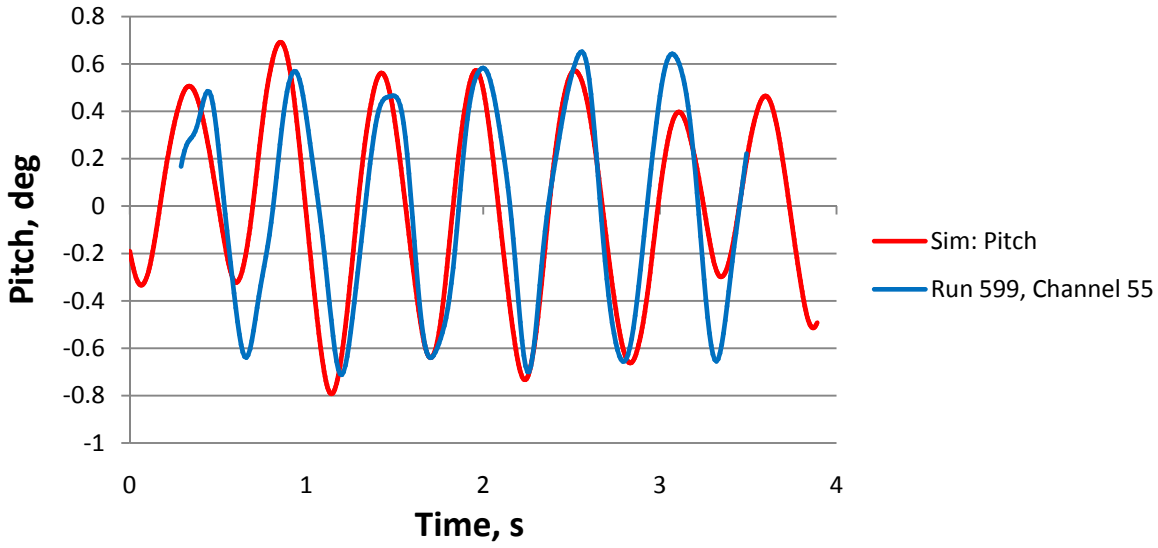

Figure 24: Pitch angle amplitude comparison, Run 599

Figures25 and 26are plots of the drag for the simulations and the model tests. Drag fluctuations for the simulations are much larger than those for the model tests. The minimum drag values from the simulations match up well with the drag from the model testing, while the maximum values are almost two or three times larger in the simulation. Notice that for both Run 599 and 601, the phases of the fulctuations from the model tests and their simulations do not agree.

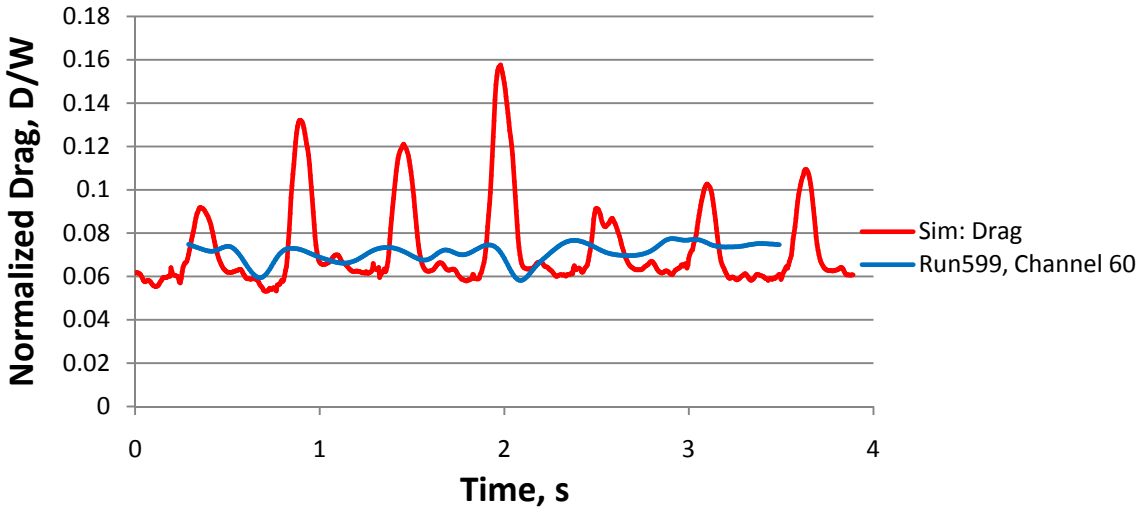

Figure 25: Drag comparison, Run 599

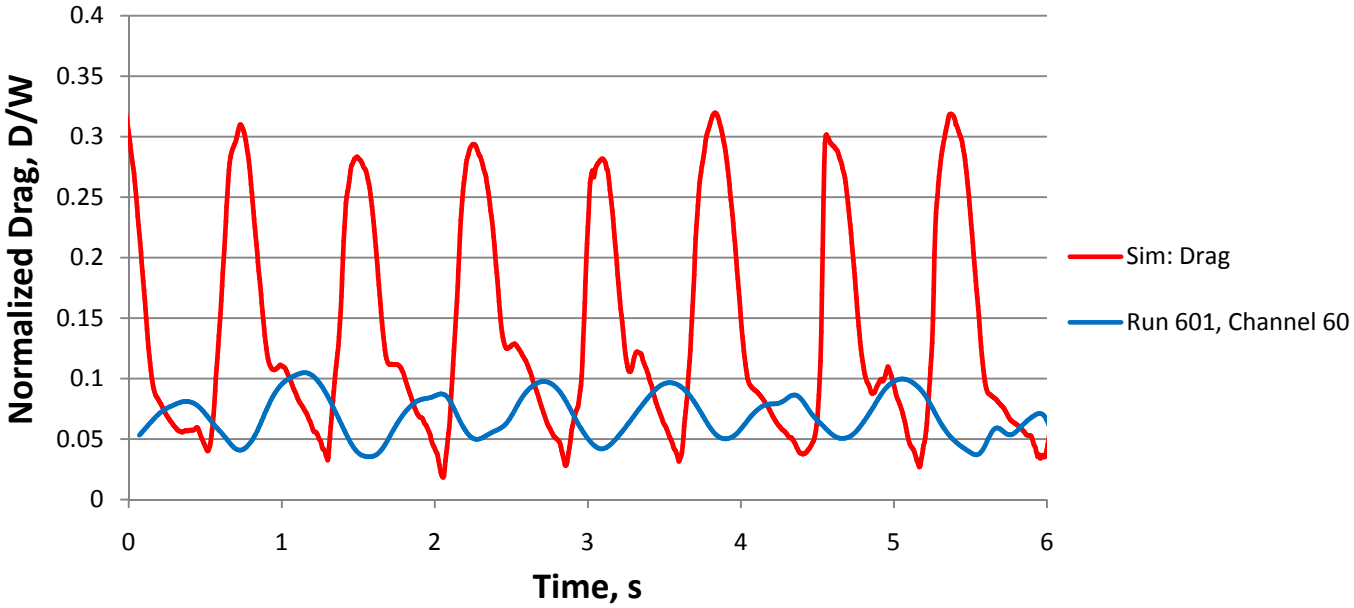

Figure 26: Drag comparison, Run 601

After examining the free surface it is clear what causes these high amplitude fluctuations in pressure, heave, and drag for the simulations of waves. As a wave approaches the bow of the craft it crashes into the rigid bow seal. This causes an intense slamming force as the water pushes against the seal. This force pushes the bow of the T-Craft up and lifts it out of the water. Figure 27 shows the volume fraction of air on the symmetry plane during these two described orientations for the simulation of Run 599. The top of the figure shows the bow down orientation with water slamming against the bow seal. The bottom shows an event where the bow has been pushed out of the water completely, reducing the drag and allowing cushion pressure to escape. As the craft's bow slams back down to the water surface, the air cushion pressure is increased and the drag spikes. The effect is more apparent in the simulation of Run 601 since the wave amplitude it almost twice that of Run 599. The dominant fluctuations in drag observed in the simulations are likely due to an effect not present in the physical model – that of the water impact on the rigid seals.

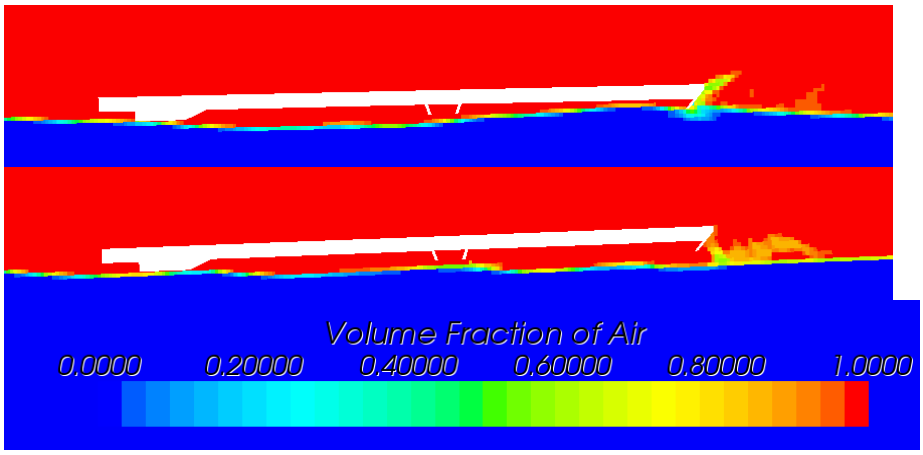

Figure 27: Volume fraction of water on symmetry plane, pitch orientations in waves, Run 599

Figures 28and29 plot the fluctuation of the drag, heave, pitch, and forward cushion pressure from their respective average values for the simulation and model test Run 599, respectively. For display purposes, the normalized drag is multiplied by a factor of 20,the pressure is divided by 200, and the heave is now plotted in centimetersrather than meters. When comparing Figures 28 and 29 it can be seen that in both the simulation and model test of Run 599, the pitch peaks and the pressure peaks occur about a half of a wavelength after the heave fluctuation peaks. The major difference between the simulation and the model test is the drag's fluctuation phase when compared to the heave and pitch. As seen in Figure 28, the drag peaks in the simulation occur slightly after the pitch fluctuation peaks. In Figure 29, it can be seen that the drag peaks for the model test occur just before the pitch fluctuation peaks.

Figure30 plots the fluctuation of the drag, heave, pitch, and forward cushion pressure from from their respective average values for the simulation of Run 601 and Figure 31 plots the fluctuation of drag and forward cushion pressure from their respective average values for the model test.For display purposes, the normalized drag is multiplied by a factor of 10,the pressure is divided by 100, and the heave is now plotted in centimetersrather than meters. In Figure 30 it can be seen that the pitch and heave peaks occur about a quarter a fluctuation wavelength apart, rather than a half of wavelength apart like for Run 599. Note that the waves in Run 601 have almost twice the amplitude and a shorter period than those of Run 599.When comparing Figures 30 and 31the major difference between the simulation of Run 601and the model test is the drag's fluctuation phase when compared to the pressure. As seen in Figure 30, the drag peaks in the simulation occur slightly after thepressure fluctuation peaks. In Figure 31, it can be seen that the drag peaks for the model test occur just before the pressurefluctuation peaks.

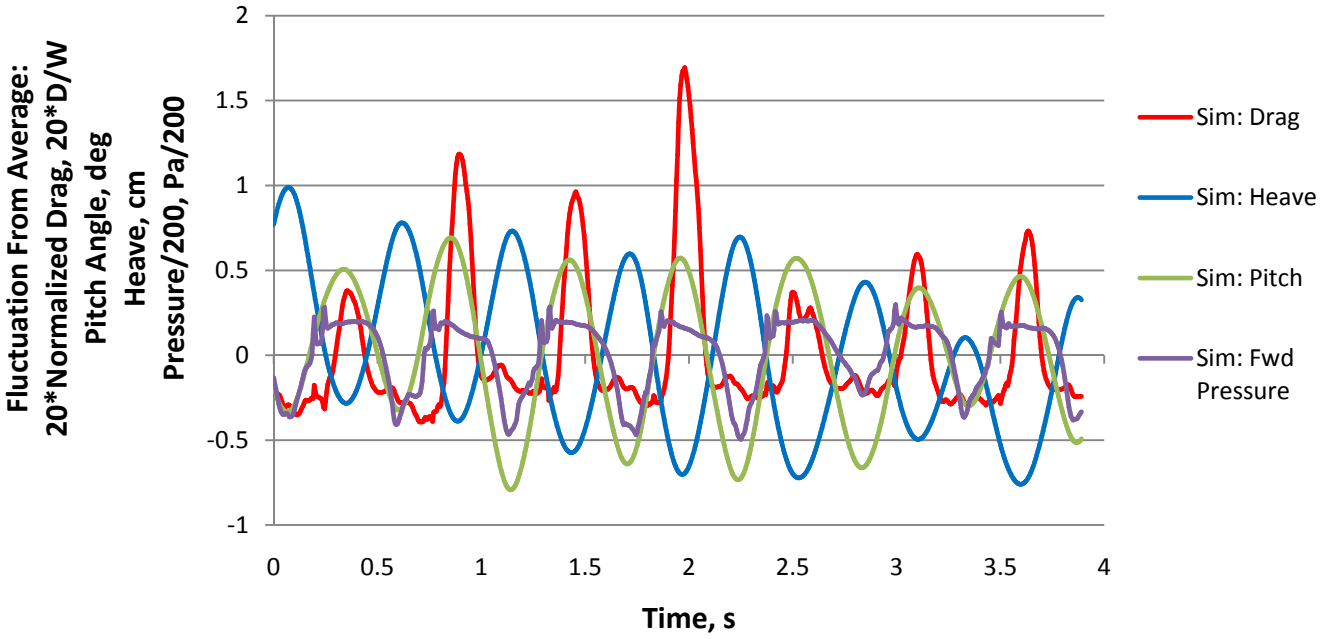

Figure 28: Drag, heave, pitch, and pressure fluctuations from average, simulation of Run 599

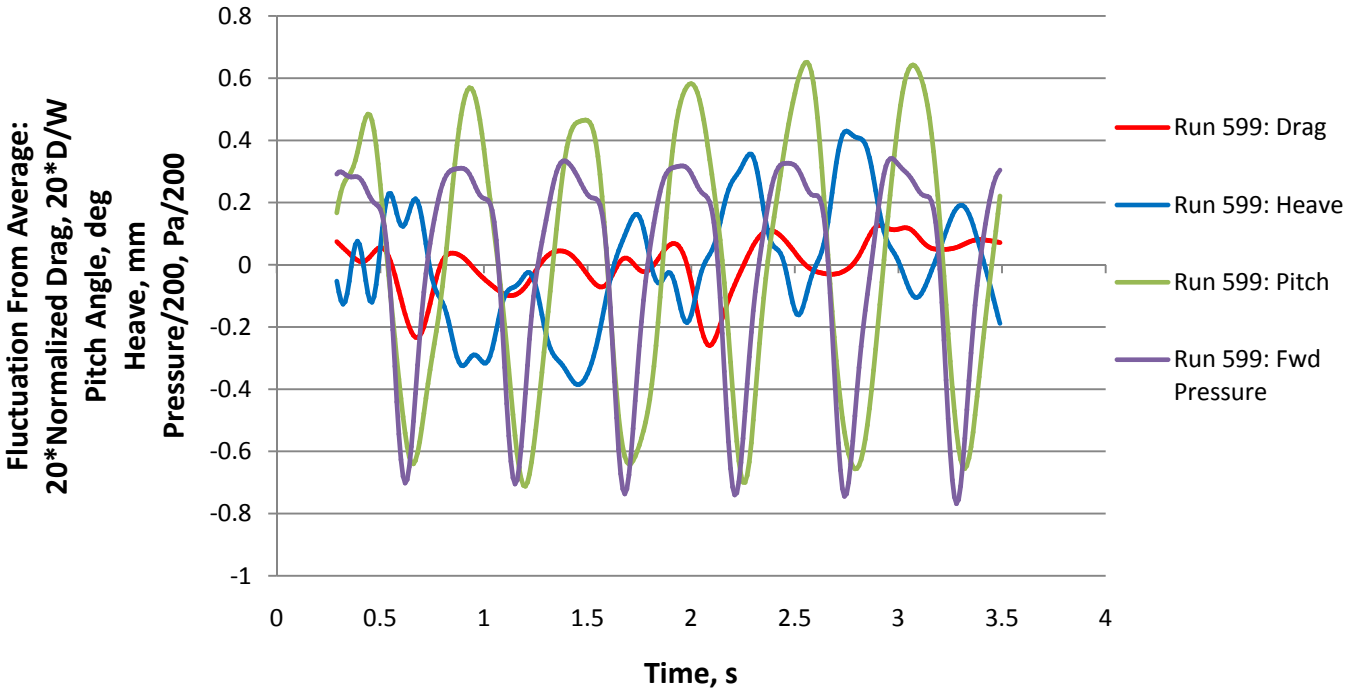

Figure 29: Drag, heave, pitch, and pressure fluctuations from average, model testRun 599

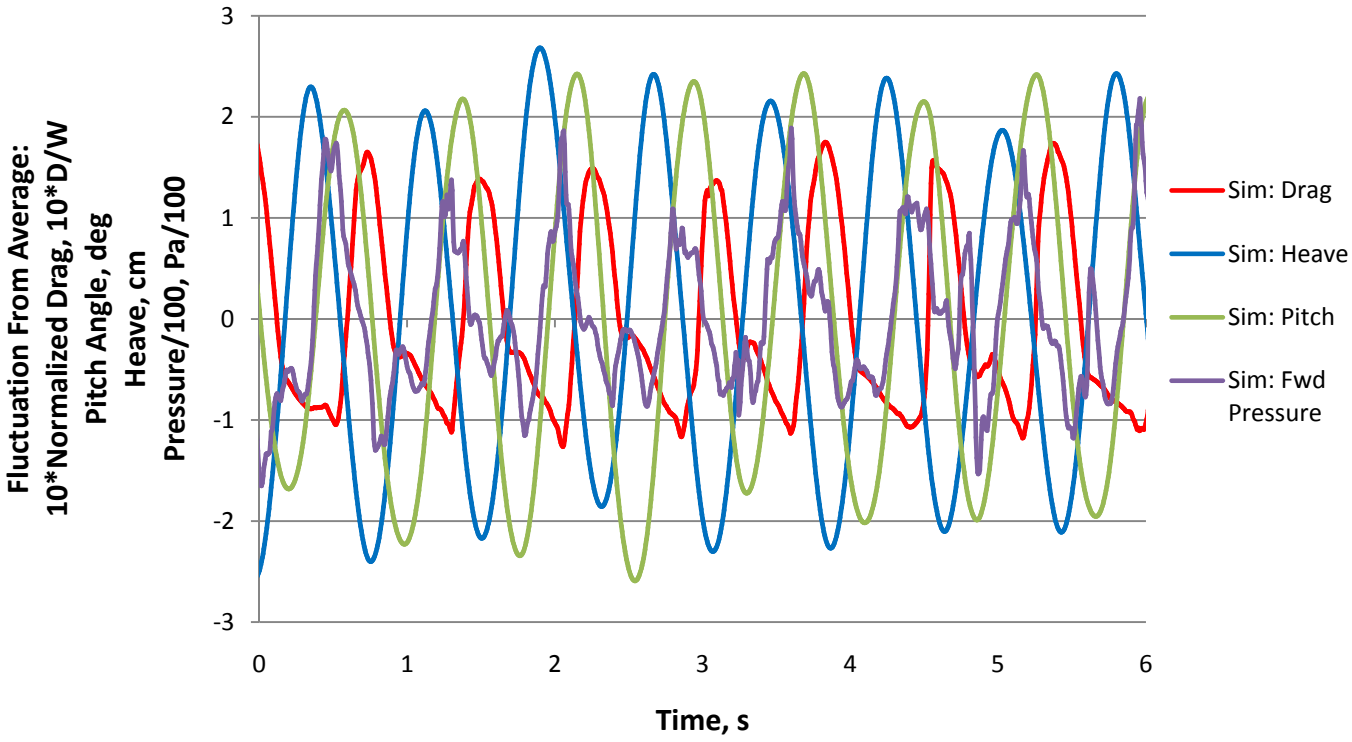

Figure 30: Drag, heave, pitch, and pressure fluctuations from average, simulation of Run 601

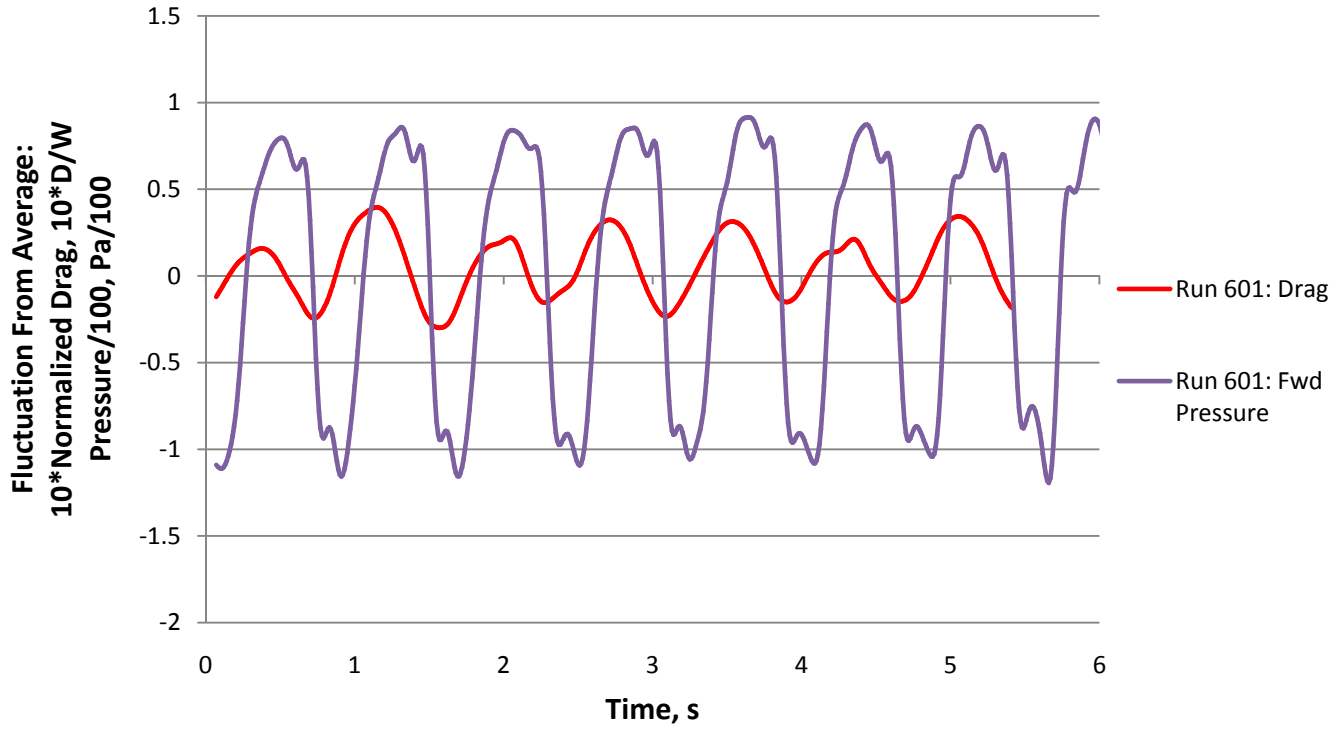

Figure 31: Dragand pressure fluctuations from average, model test Run 601

5.2 Further Inviscid Simulation

In an attempt to examine the free surface response induced by the air cushion at speeds approaching and passing the air cushion wavemaking drag hump speed, discussed above, Froude numbers other than those used in model testing were simulated. Constant-velocity, inviscid simulations of Froude numbers ranging from 0.05 to 1.1 in 0.05 increments were carried out. A simulation with a third degree of freedom in the surge direction was also performed. In this simulation, the T-Craft model starts at rest and accelerates to a Froude number of 1.1. This is done by the application of an80 Newton or 18 lb, (40 N for half model with symmetry) constant force at the center of mass of the craft.The seals for all of these simulations are shortened to the same length, the same as Froude number of 0.2 configuration "Seals 2" and the Froude number of 0.6 configuration "Seals 1".

The drag values for these runs as well as for the model tests compared to Froude number are presented in Figure 32. The drag values for each of the different simulations share a common trendline. The constant force simulation shows two considerable spikes in the drag at a Froude number of about 0.6 and 0.85. Investigation of a video of the free surface underneath the air cushion reveals that at the Froude number of 0.6 drag spike, the internal wave has grown to the length to the air cushion and the crest of the wave is hitting the rigid aft seal. The drag spike at a Froude number of 0.85 is attributed to the widening crest generated at the bow of the craft expanding into the rigid transverse seal. Figure 33 shows free surface elevation contours with the T-Craft removed at these two Froude numbers. Other deviations of the constant force simulationfrom the constant velocity simulations, such as the increased drag at Froude numbers below 0.2 and the drag dip at a Froude number of 0.7, may be caused by acceleration effects. For the majority of the Froude numbers the constant velocity simulation drag and the constant force simulation drag match very well.

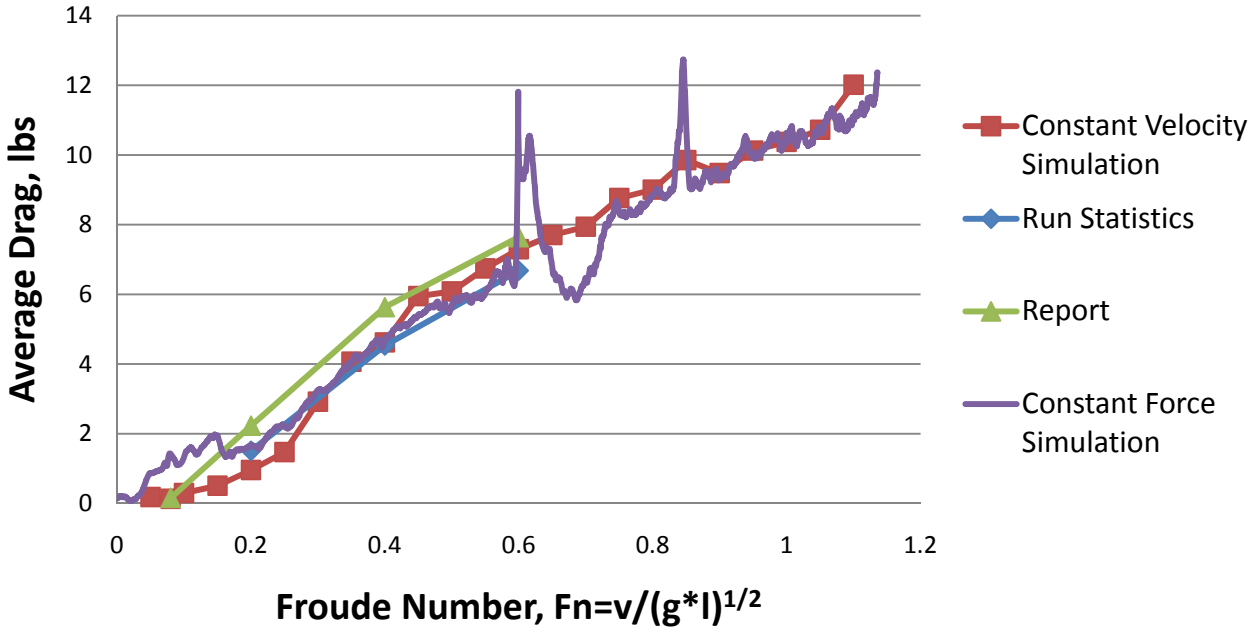

Figure 32: Drag versus Froude number for constant velocity simulations and constant force simulation

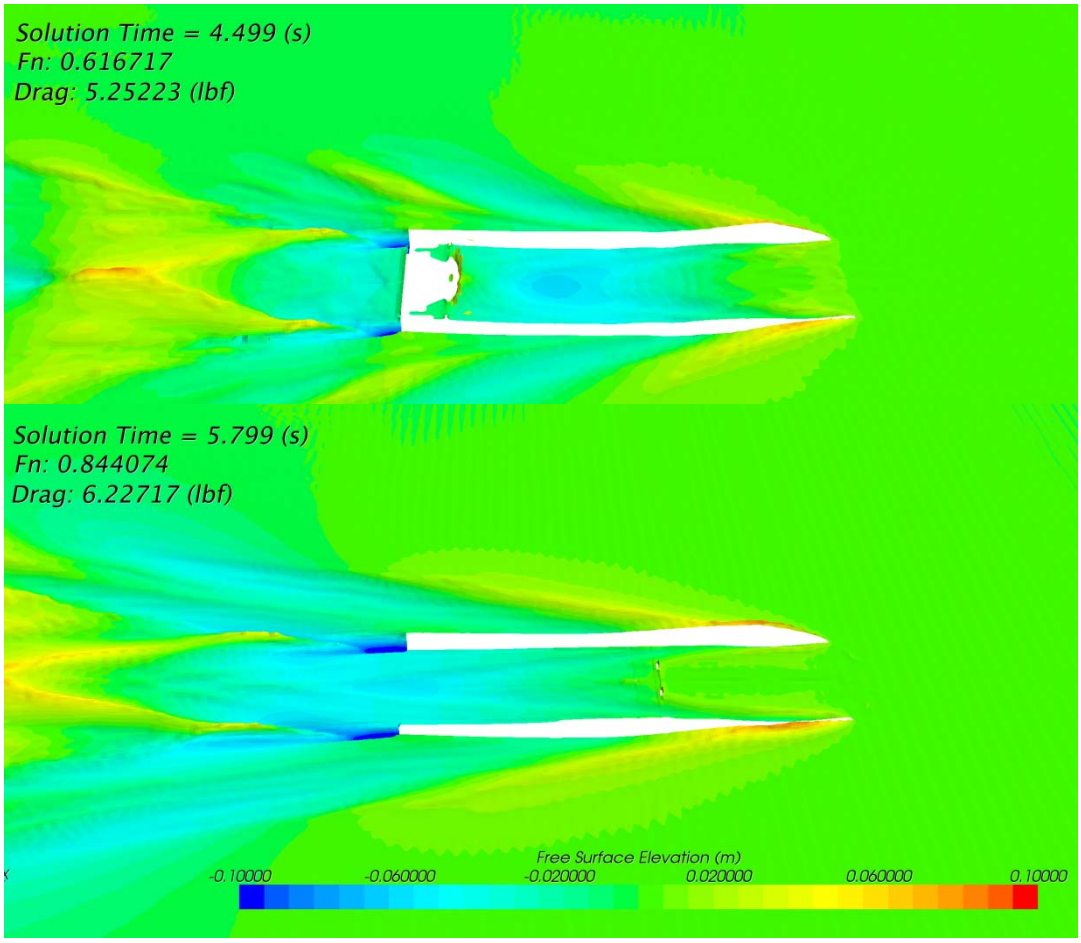

Figure 33: Free surface elevation contours for constant force simulation at drag spikes

Free surface elevation contours from constant velocity simulations of Froude numbers 0.1 to 1.1 in 0.1 increments are presented below in Figures34-36. When comparing the free surface contours it is clear that the wavelength of the wave internal to the hull gradually increases with speed. At lower Froude numbers there are many wavelengths internal to the hull which would have a lot of interaction with the seals in reality. No drastic changes in the free surface are apparent as the craft approaches the air cushion wavemaking drag hump speed of about a Froude number of 0.8. It can be seen however, that at speeds above a Froude number of 0.8, the wave trough from the wave started internally has moved to behind the craft and the entire craft is riding on the bow-up slope of the wave crest started at the bow. At these speeds above the hump speed, the craft is riding on less than one quarter of the generated wave's wavelength.

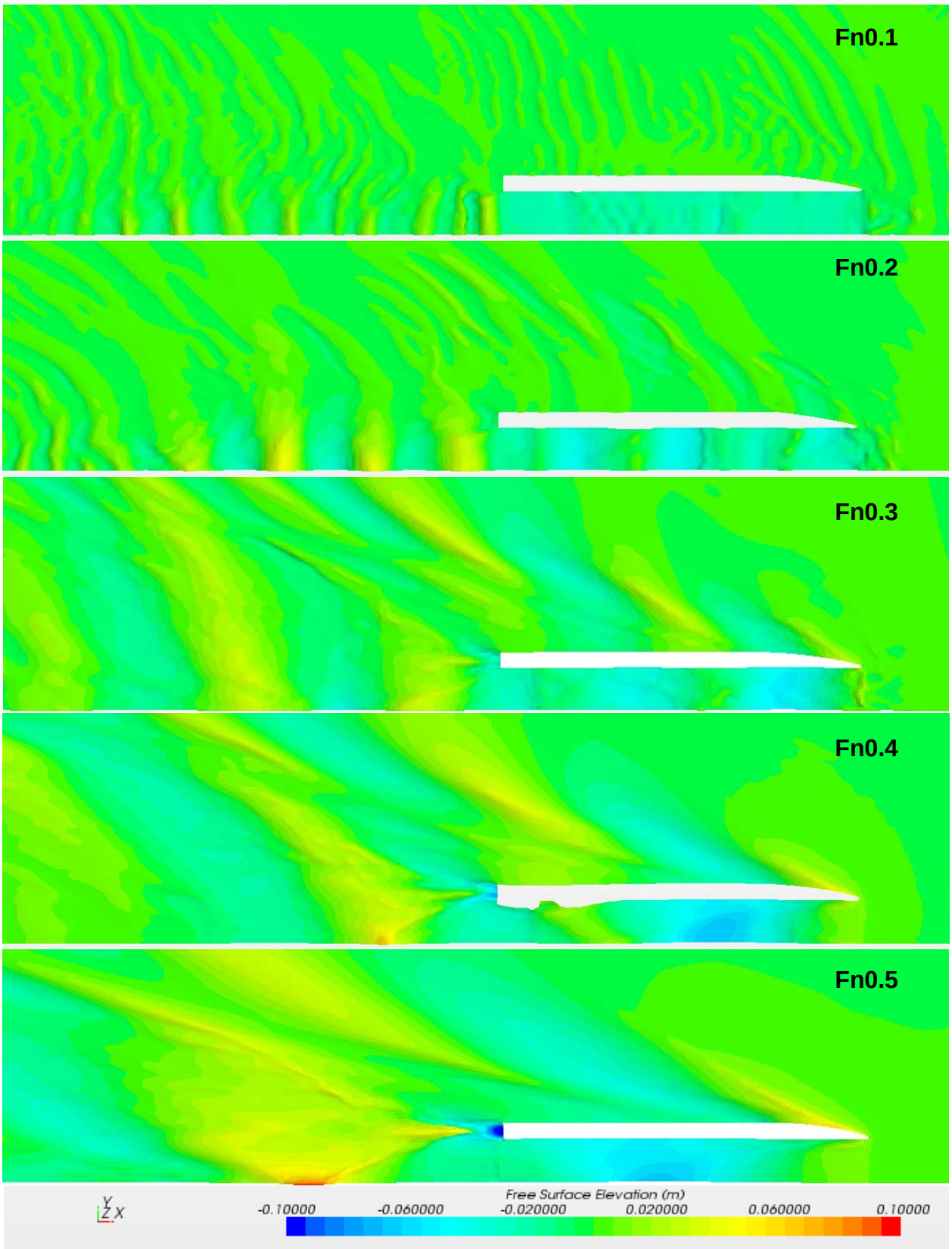

Figure 34: Free surface elevation contours, Fn 0.1-0.5

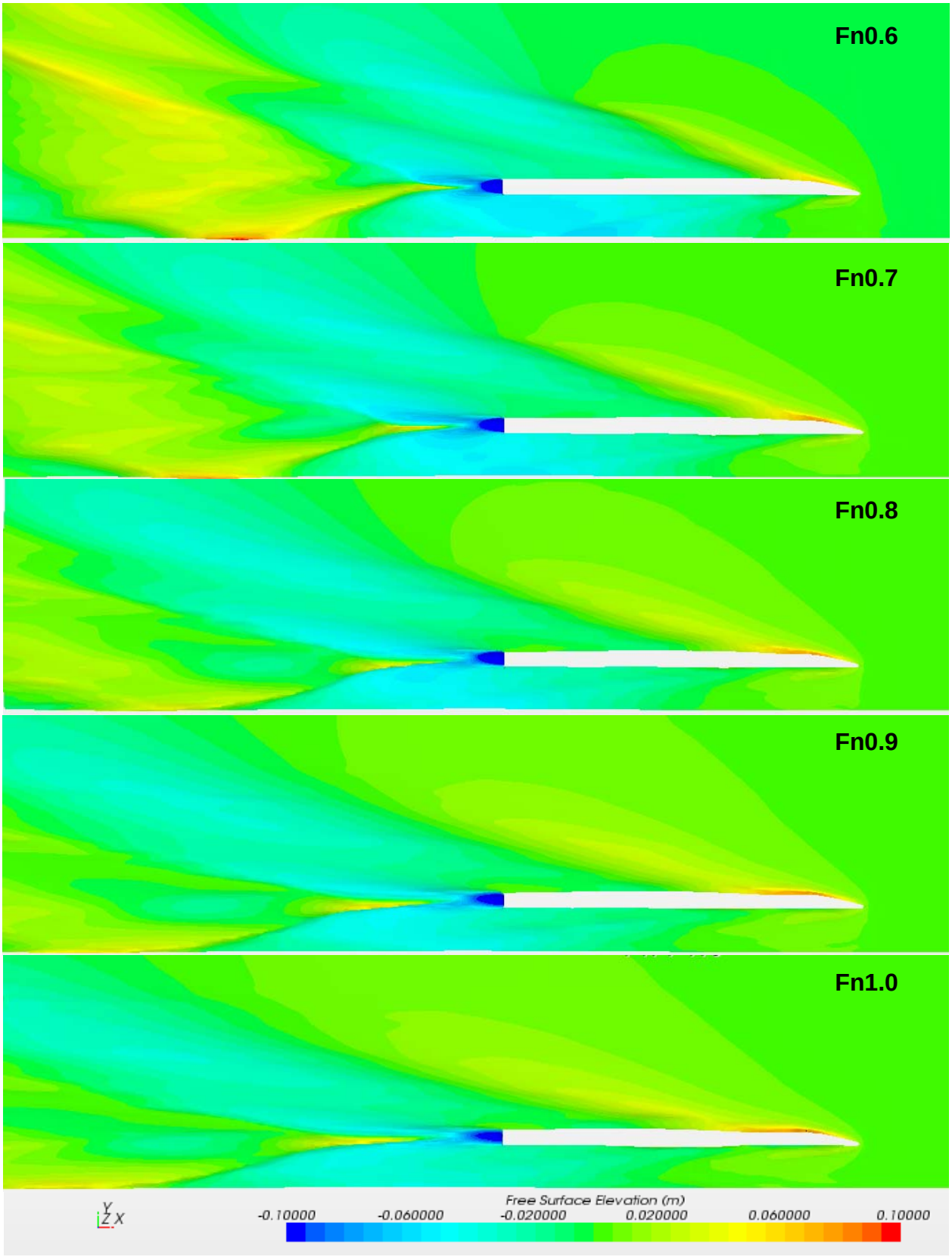

Figure 35: Free surface elevation contours, Fn 0.6-1.0

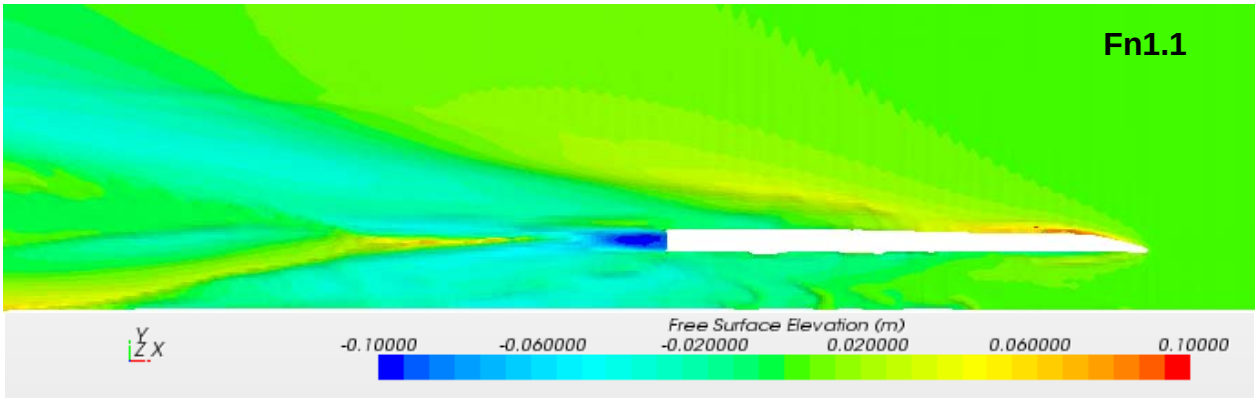

Figure 36: Free surface elevation contours, Fn 1.1

5.3 Viscous Simulation

To investigate the effects of viscosity and turbulence on the simulation's results, viscous simulations of the model tests were also conducted. The turbulence model used is the Spalart-Allmaras turbulence model which solves a single transport equation to determine the turbulent viscosity. For these simulations, the drag is broken up into components to give a better understanding of the simulations' accuracy and the effect of the rigid seals. The drag components calculated include both the shear and pressure drag caused by both the air and the water for the hull and each of the seals. To examine the effects of viscosity, each of the viscous simulations were re-calculated with viscosity turned off, using the same mesh for better comparison. To reduce the time dependent effects from pitch and heave movements and to help generate better free surface elevation contours for comparison, each simulation was run with no degrees of freedom at the average pitch and heave orientation for both simulations with viscosity and inviscid simulations. The orientations used in each of the 0-DOF simulations are given in Table 3. Convergence issues with the inviscid simulation of Froude number of 0.4with 2-DOF prevented an orientation to be determined so the orientation from the viscous 2-DOF simulation is used. As can be seen, some differences emerge from the inviscid and viscous simulations' average orientation, but these differences are as small as millimeters and hundredths of a degree.

0-DOF Simulation Orientations				
	Viscous		Inviscid	
Froude Number	Heave (m)	Pitch (deg)	Heave (m)	Pitch (deg)
0.08	0.00713	-0.299	0.00578	-0.315
0.2	0.00822	-0.455	0.00667	-0.394
0.4	0.000153	-1.25	0.000153*	-1.25*
0.6	-0.00354	-1.64	-0.00505	-1.67

Table 3: 0-DOF simulation orientations

Figure 37 shows some of these viscousdrag components compared to the total inviscid drag and model test results from the report. The total drag from the simulations with viscosity is overestimated in the Froude number of 0.08, 0.4, and 0.6 simulations but was underestimated for the Froude number of 0.2 simulation. The underestimation may be due to the shortened rigid skirts that are not interacting with the numerous internal waves produced under the air cushion. Despite these inaccuracies, the viscous simulations' total drag values are closer to the model test drag values than the inviscid

simulations' total drag values. The drag on each of the seals remains relatively constant through the range of Froude numbers. The drag due to the water on each of these seals is basically zero, ensuring a gap between the seal and the free surface. Because of this the majority of the seal drag is due to the pressure drag due to the air from the air cushion. This explains why the bow seal has negative drag, as the pressure from the air cushion acts on the rigid seal's interior face in the opposite direction of drag forces. The transverse seal has nearly equal pressures pushing on it in opposite directions from the fore and aft air cushions, leaving a total drag of nearly zero. The aft seal has an almost equal drag value as the bow seal, but in the opposite direction giving positive drag. The pressure from the air cushion acts and escapes from the bow seal in the opposite direction of travel, causing a positive drag. In reality the total seal drag would be positive as the seals would drag in the water.

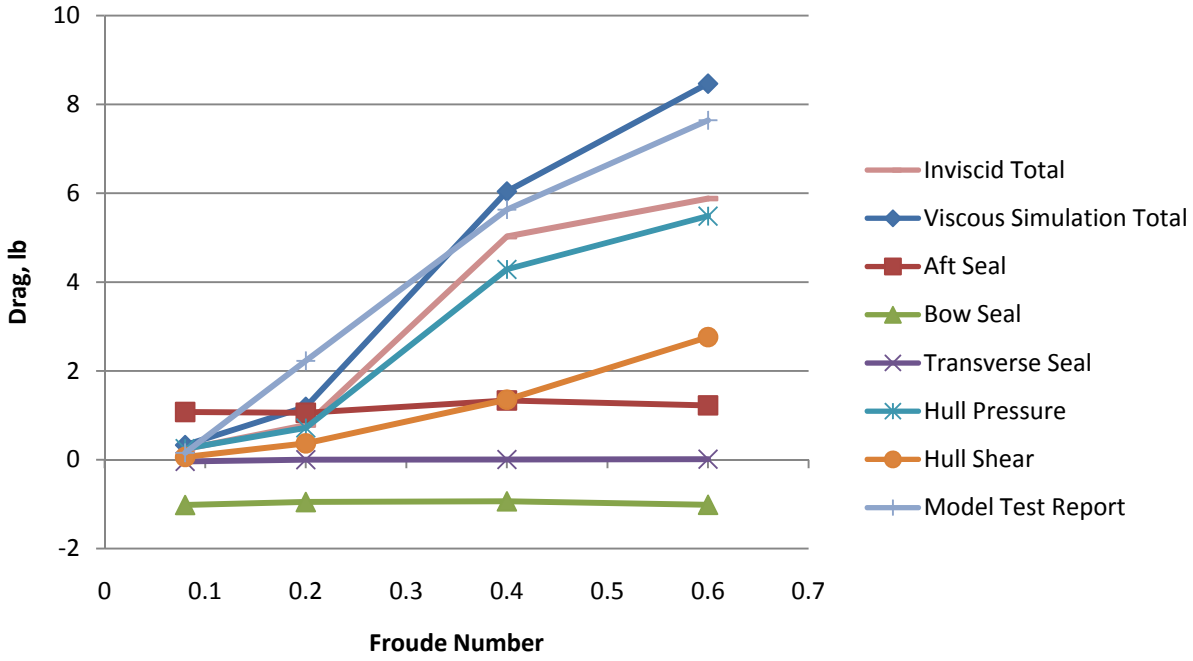

Figure 37: Drag comparison and viscous simulation drag components

Figure 38 shows more of the drag components from the simulations with viscosity. It can be seen that the drag due to air shear and the seals are close to zero for all of the simulations. While the majority of the drag is composed of the pressure drag due to the water and air, the water shear drag makes up about 25% of the total drag for each of the simulations. This shows how not calculating shear drag in inviscid simulations can be a large source of error.Air pressure drag was also found to be positive in the inviscid simulations and is due to the air cushion pressure acting on the underside of the craft while in a bow-up orientation. Figure 39 compares the calculated water shear drag from the viscous simulations, the difference between the total drag from the viscous and inviscid simulations, and the calculated water shear drag using the ITTC-1957 frictioncoefficient line for shear drag using the wetted surface area from a zero-velocity simulation. Adding the ITTC-1957 friction coefficient line shear drag to the total drag from the inviscid simulations yields drag values close to the viscous simulations' total drag values, with the largest difference being 6% for the Froude number of 0.08 simulations. The water shear drag calculated from the viscous simulations is slightly less than that calculated using the ITTC-1957friction coefficient line for all Froude numbers, the difference for the Froude number of 0.6 case is only 7% .

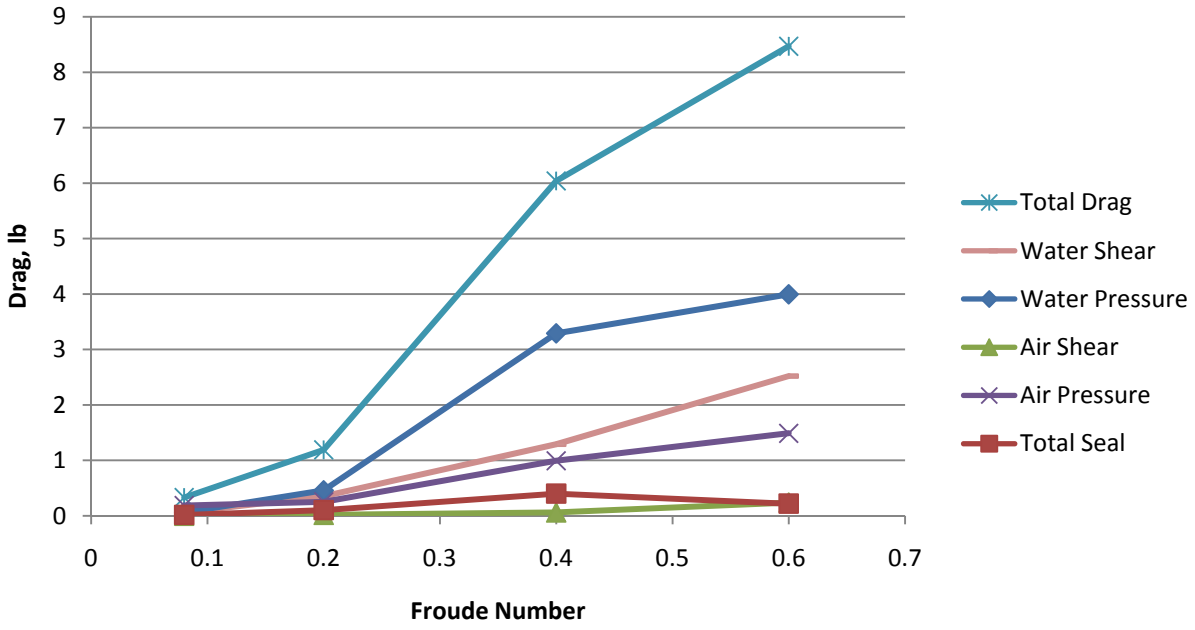

Figure 38: Viscous drag components

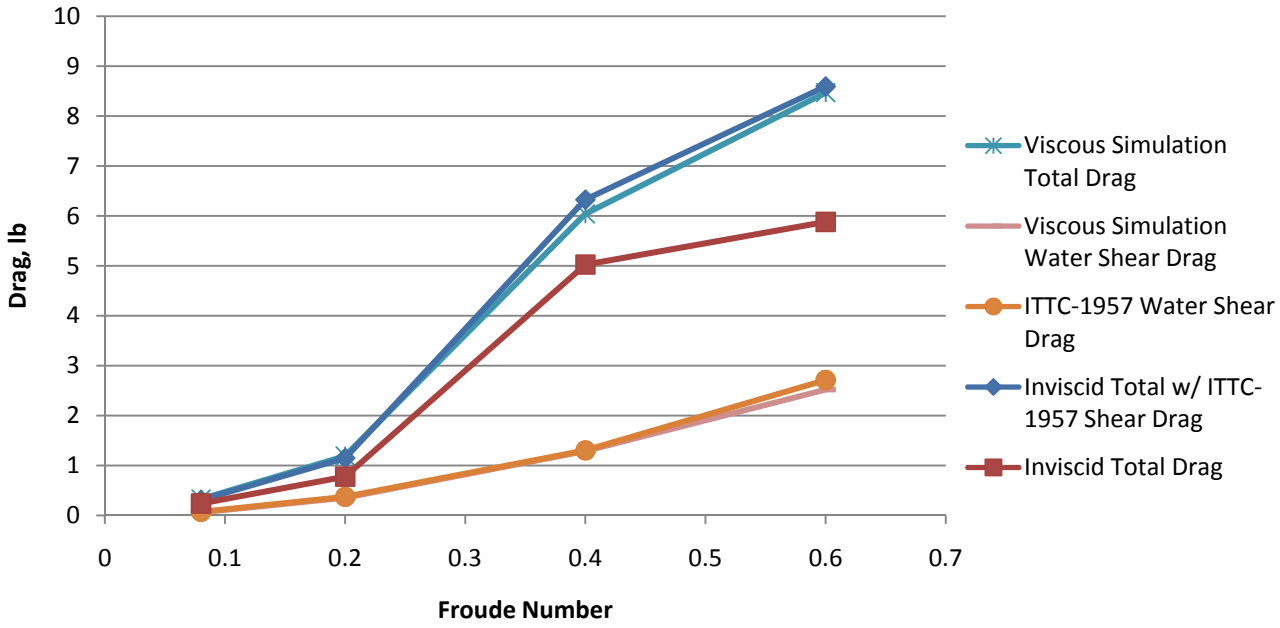

Figure 39: ITTC-1957 friction coefficient line shear drag comparison

Free surface elevation contours from these simulations are presented in Figures 40 and 41 for comparison. It can be seen that the free surface shape is very similar between inviscid and viscous simulations. When comparing the Froude number of 0.08 simulations it can be seen that the waves generated in the inviscid simulation are more pronounced. The waves seem to start closer to the bow of the craft and their amplitude is larger behind the craft in the wake. For the inviscid Froude number of 0.2 simulations, the waves appear to be more choppy and their amplitude is greater, particularly to the sides of the craft.The reduced amplitudes in the simulation with viscosity can be attributed to viscous damping.Much less difference can be seen between the Froude number of 0.4 simulations. The

biggest difference is the interaction with the stern seal. Since these simulations are still time dependent, this interaction may change with time. When comparing the Froude number of 0.6 simulations, it can be seen that the bow wave is slightly larger for the inviscid simulation while the amplitude of the wake behind the craft is slightly larger in the viscous simulation. While some differences can be seen between the viscous and inviscid simulations for each Froude number, the same flow features and wake patterns are present in both simulation types.

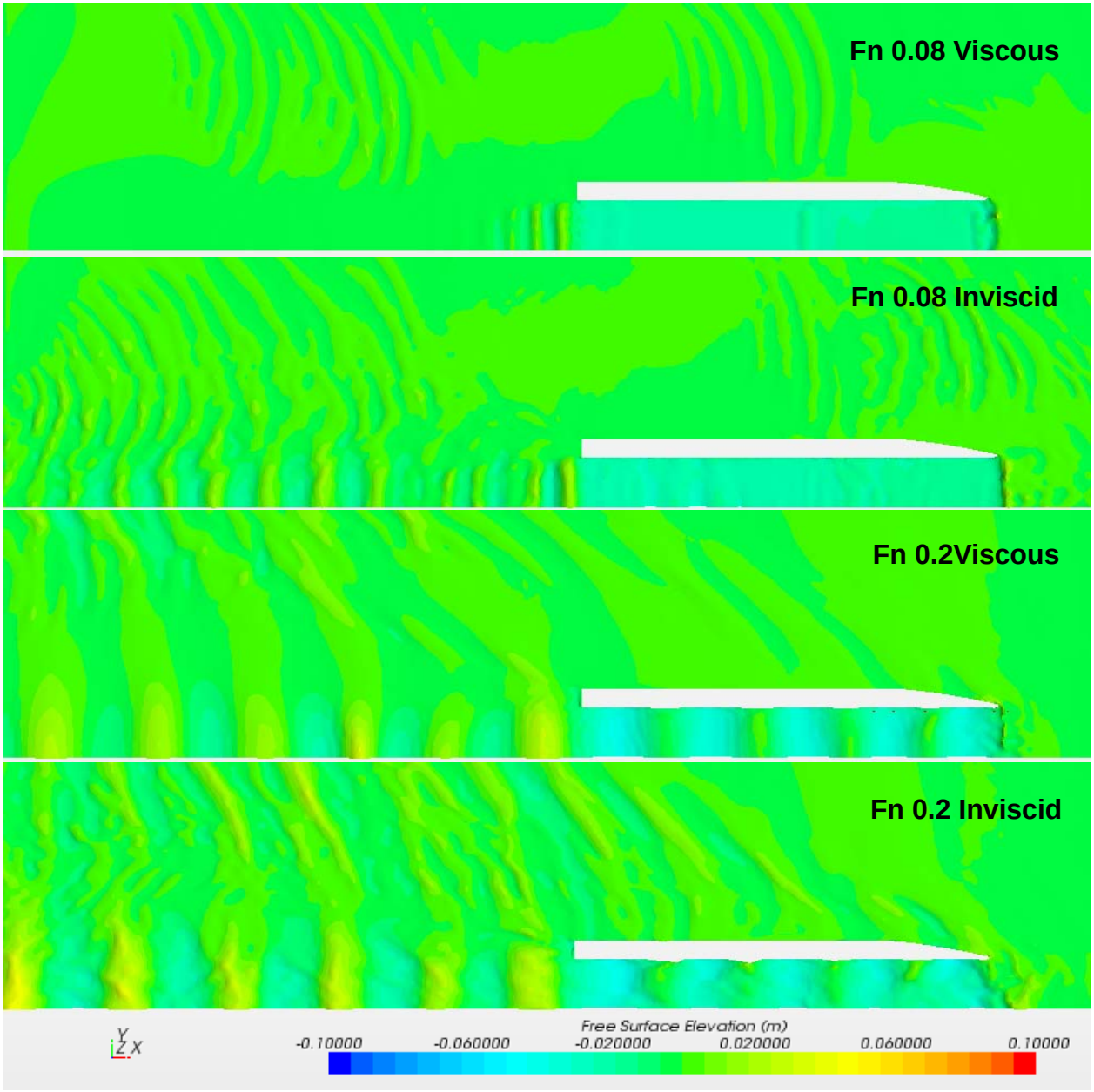

Figure 40: Free surface elevation contours, Fn 0.08 and Fn 0.02

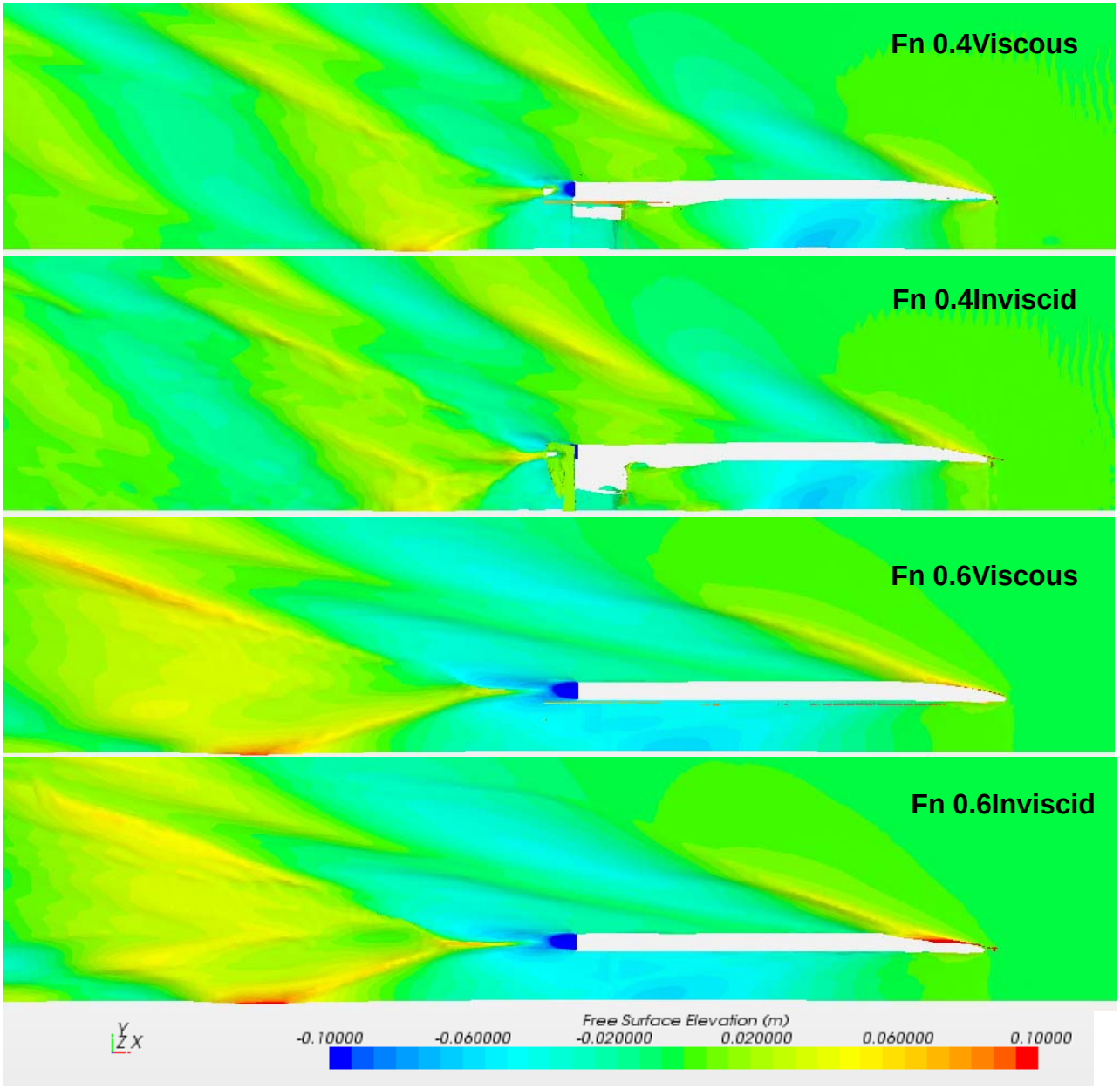

Figure 41: Free surface elevation contours, Fn 0.4 and Fn 0.6

The 3-DOF simulation with a constant applied force was also simulated with viscosity. Figure 42 shows the drag and drag components from this simulation compared to the drag data from the inviscid simulation discussed earlier. The drag data from both simulations share a similar trend and the predominant drag spike at a Froude number of about 0.6. The aft seal drag monitor from the viscous simulation confirms that this drag spike is caused by water hitting the aft seal. The viscous simulation's drag does not show the same drag spike due to the transverse seal at a Froude number of 0.85, but the transverse seal drag monitor shows a positive drag starting around this Froude number. The calculation of viscous forces adds a considerable amount of shear drag to the total drag, especially as speed is increased. When examining the hull pressure drag from the viscous simulation, the air cushion wavemaking drag "hump", discussed earlier, can be seen around a Froude number of 0.8. The hull pressure drag monitor neglects forces on the seals and only calculates the pressure drag on the hull. Although the pressure drag on the hull does not only include the wavemaking drag due to the air cushion, but also the wavemaking drag due to the sidehulls, the effect of the air cushion

wavemakingdrag humpis still apparent. At a Froude number of 0.8 an air cushion of this length to beam ratio meets its maximum wavemakingdrag and the drag decreases as speed is increased.

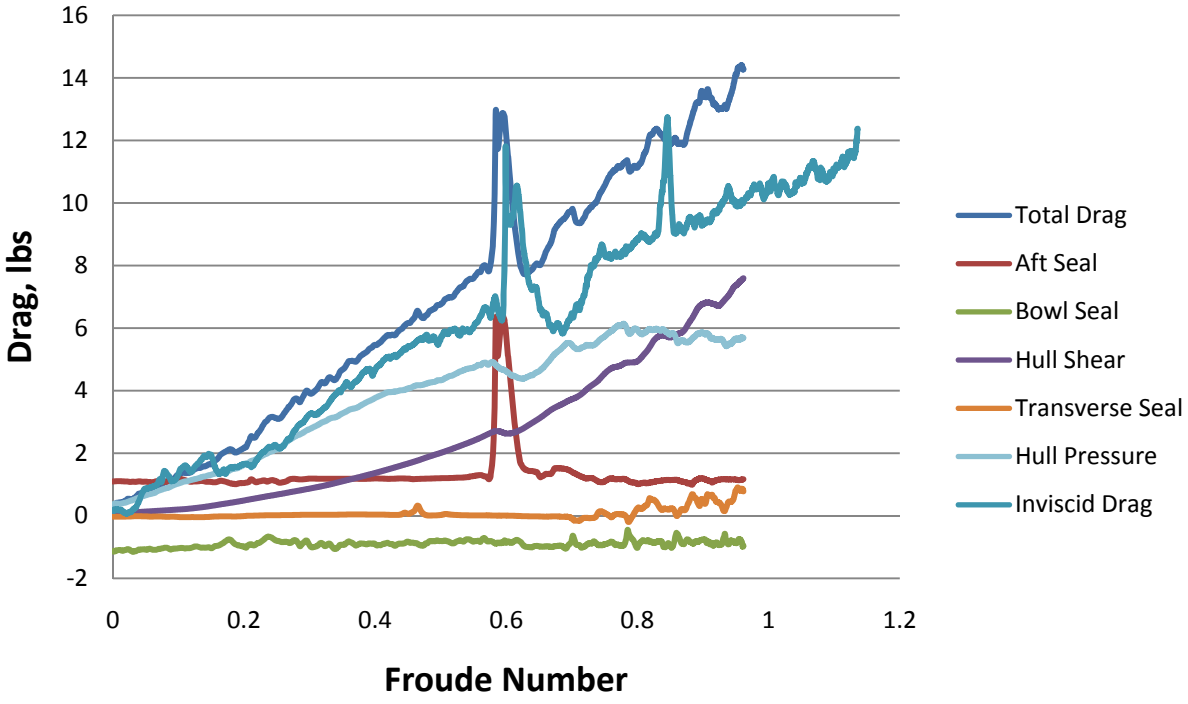

Figure 42: 3-DOF simulation drag components comparison

5.4 Qualitative Comparison of Results

During the model tests at NSWCCD, video was taken of the each run from four angles. The craft can be viewed from the port stern quarter, the bow port quarter, the starboard side, and from above. Although the footage is zoomed in tight to the model and doesn't have the best lighting or quality, some flow features are still distinguishable. Figures 43through 50 compare free surface elevation contours from the viscous and inviscid simulations to stills from the model testing video. Figures 43 and 44 are of the Froude number of 0.08 test, Figures 45 and 46 are of the Froude number of 0.2 test, Figures 47 and 48 are of the Froude number of 0.4 test, and Figures 49 and 50 are of the Froude number of 0.6 test. For all of the figures, the free surface elevation from the viscous case is presented on the top while the contours from the inviscid case are on the bottom.

Only two dominant flow features can be clearly seen from the video of the Froude number of 0.08 model test. These are of the choppy wake behind the model and transverse waves that seem to form around the midship. The viscous simulation seems to reproduce the transverse waves on the sides of the model more accurately than the inviscid simulation. In the inviscid simulation they seem to form much closer to the bow of the craft and have larger amplitudes. The wake behind the craft seems more chaotic in the inviscid simulation and seems to match the video better.

The video reveals more of the wake at the higher Froude numbers. Five transverse waves can be seen along the length of the hull in the Froude number of 0.2 model test video. The same number of transverse waves can be seen in both the inviscid and viscous simulations, however the inviscid

simulation's waves are more pronounced. The wake behind the craft in the video also appears to match those from the viscous and inviscid simulations.

For the Froude number of 0.4 case almost two wavelengths of transverse waves can be seen along the length of the craft in the video and in both the viscous and inviscid simulation. Not much difference can be seen between the viscous and inviscid simulations. The amplitude of the wake directly behind the side hull is more exaggerated in the inviscid solution.

Only about one and a half wavelengths of transverse waves can be seen along the length of the craft at a Froude number of 0.6 and the wake becomes tighter. This can be seen in the video and in both the inviscid and viscous simulations. Both simulations seem to exaggerate the height the water travels up the bow. For all of the Froude numbers the free surface elevation contours from both the inviscid and viscous simulations share similar wake patterns with those captured in the model testing videos.

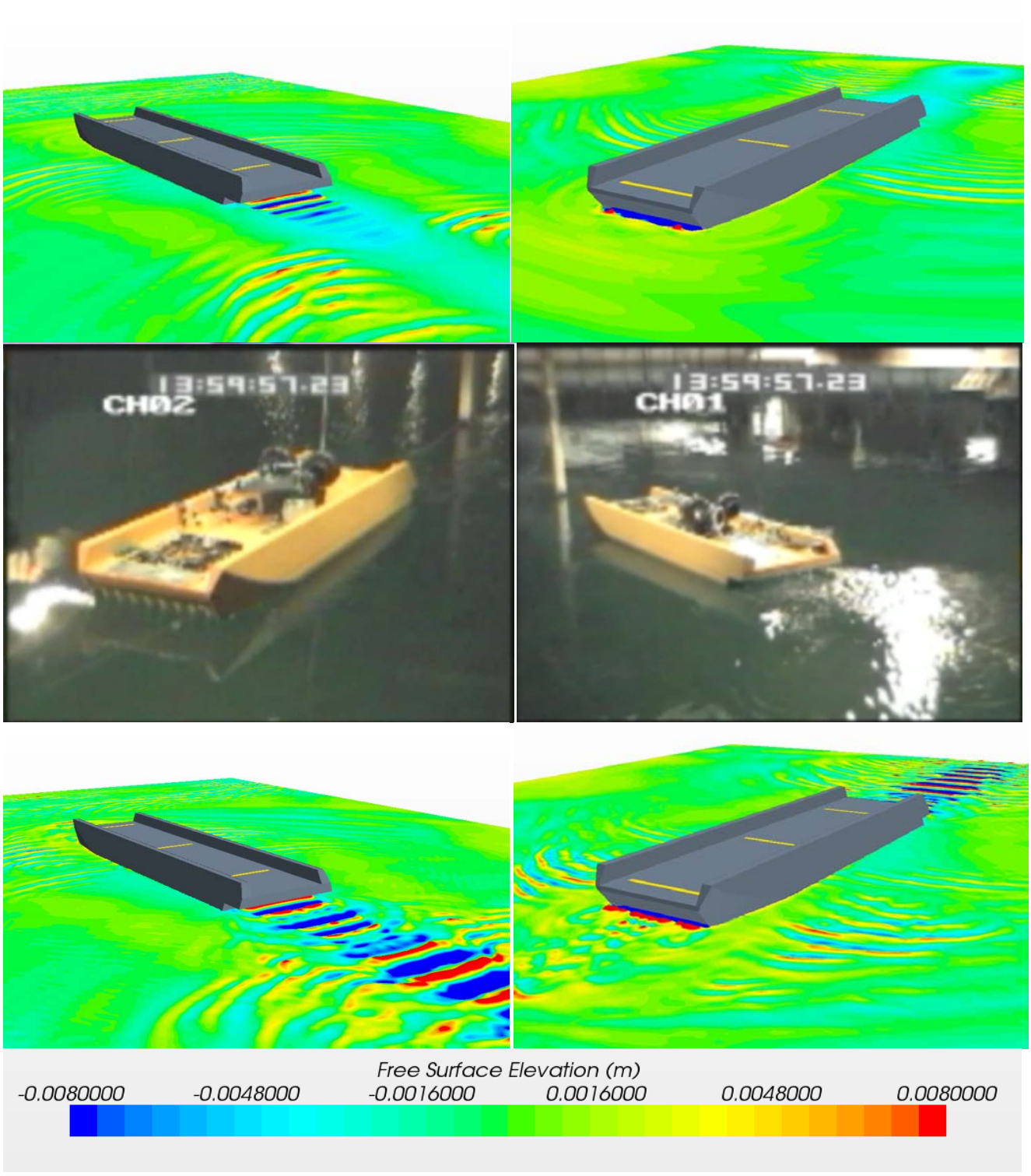

Figure 43: Free surface, Fn 0.08, Top: viscous simulation, Bottom: inviscid simulation

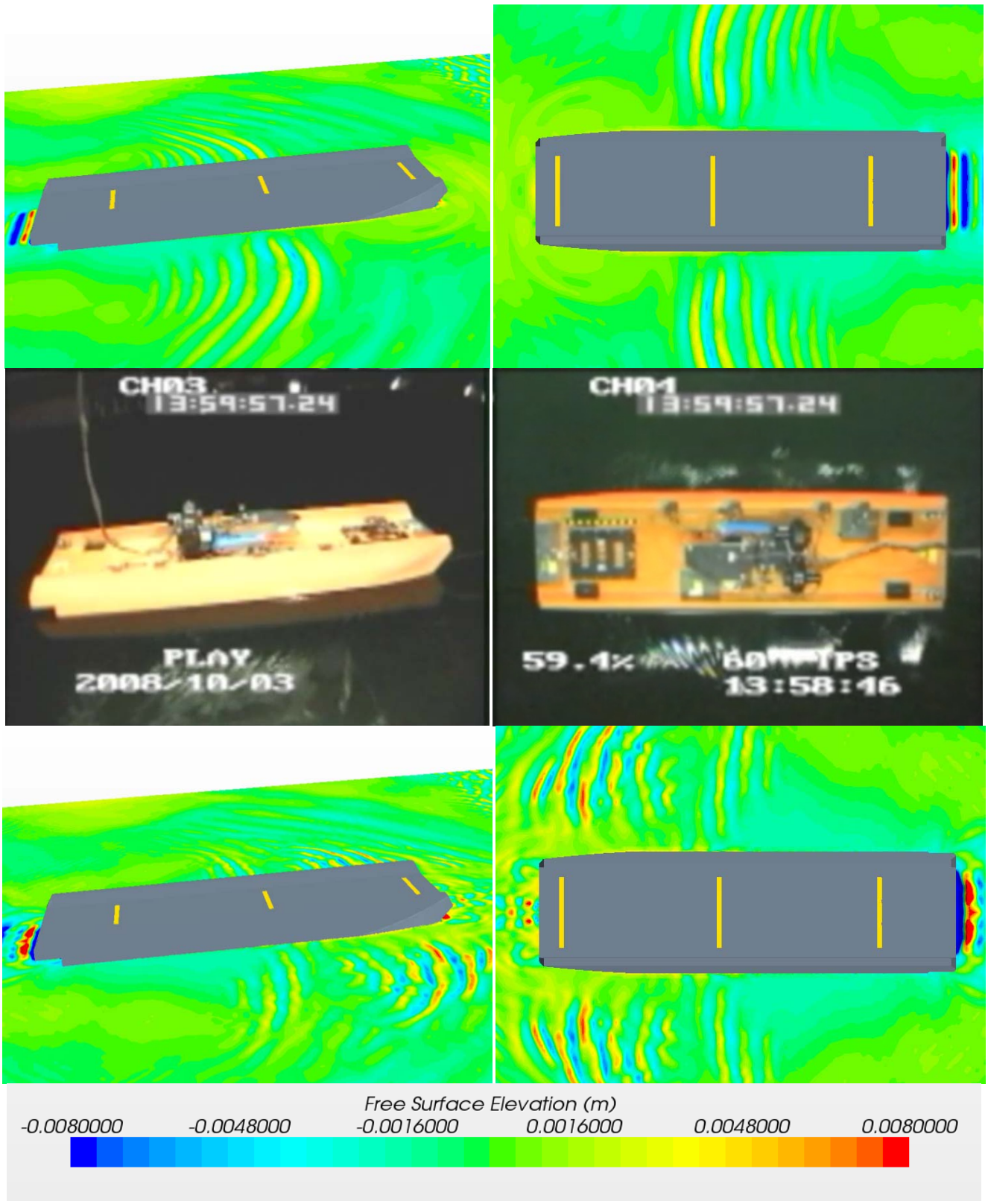

Figure 44: Free surface, Fn 0.08, Top: viscous simulation, Bottom: inviscid simulation

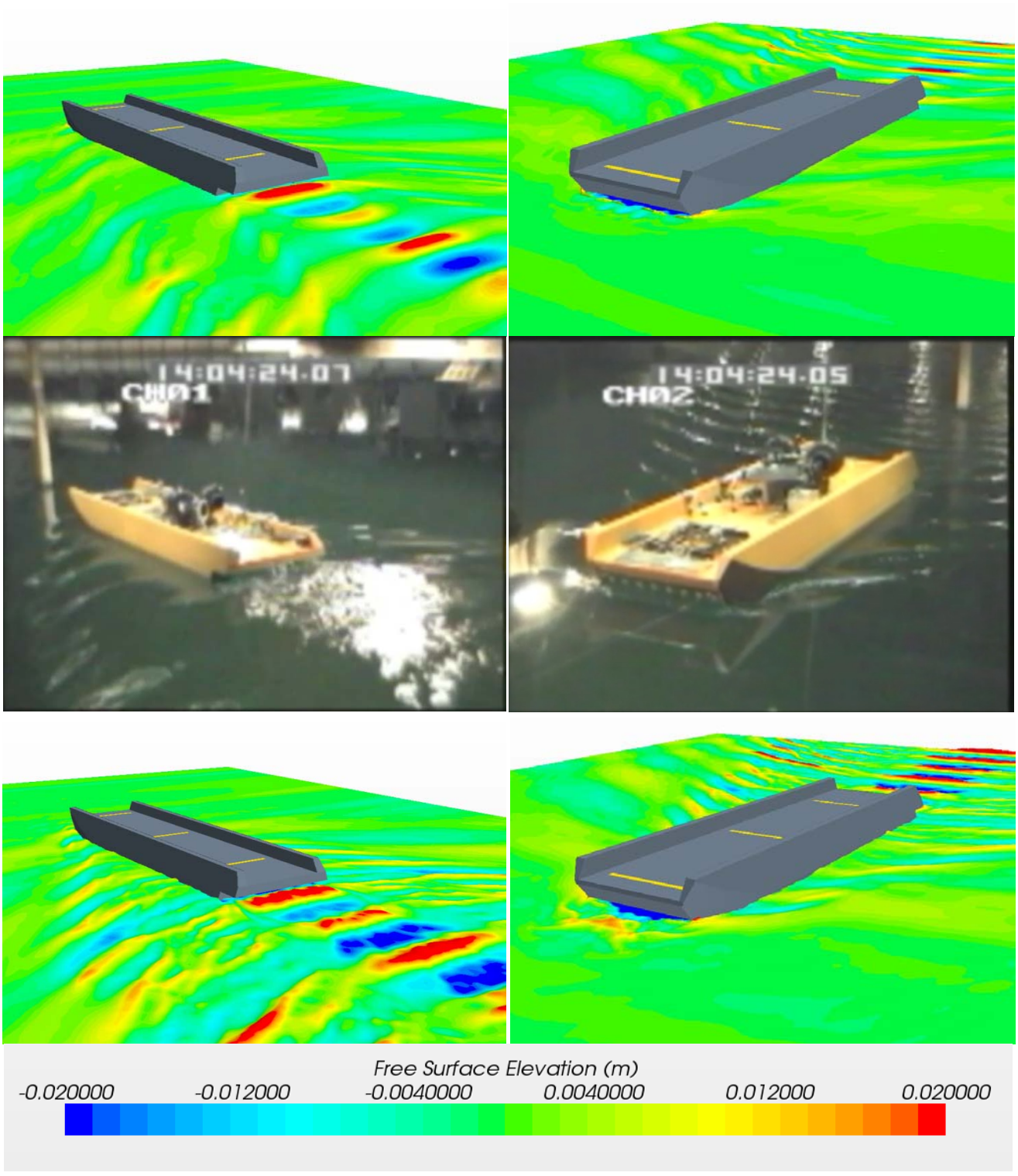

Figure 45: Free surface, Fn 0.2, Top: viscous simulation, Bottom: inviscid simulation

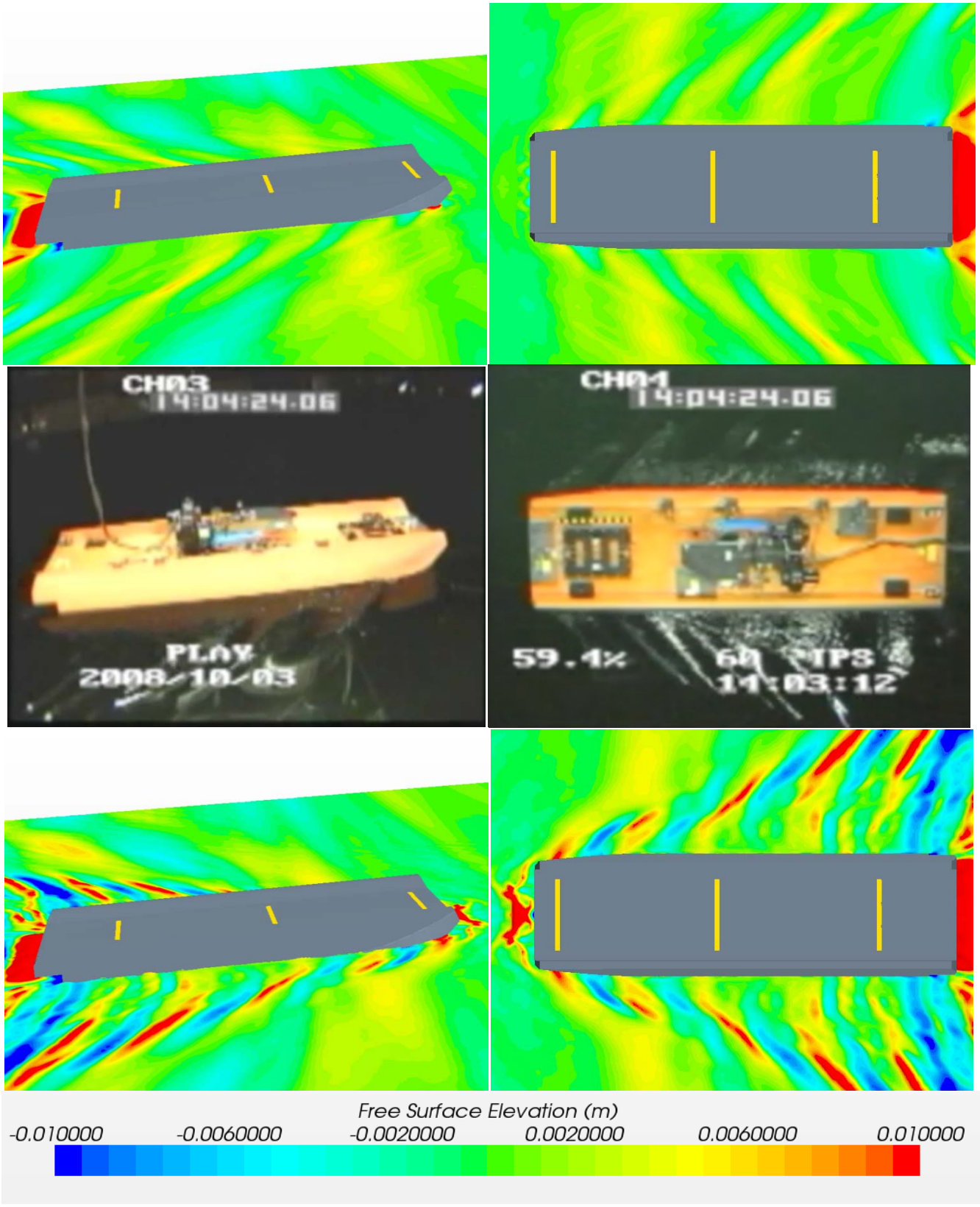

Figure 46: Free surface, Fn 0.2, Top: viscous simulation, Bottom: inviscid simulation

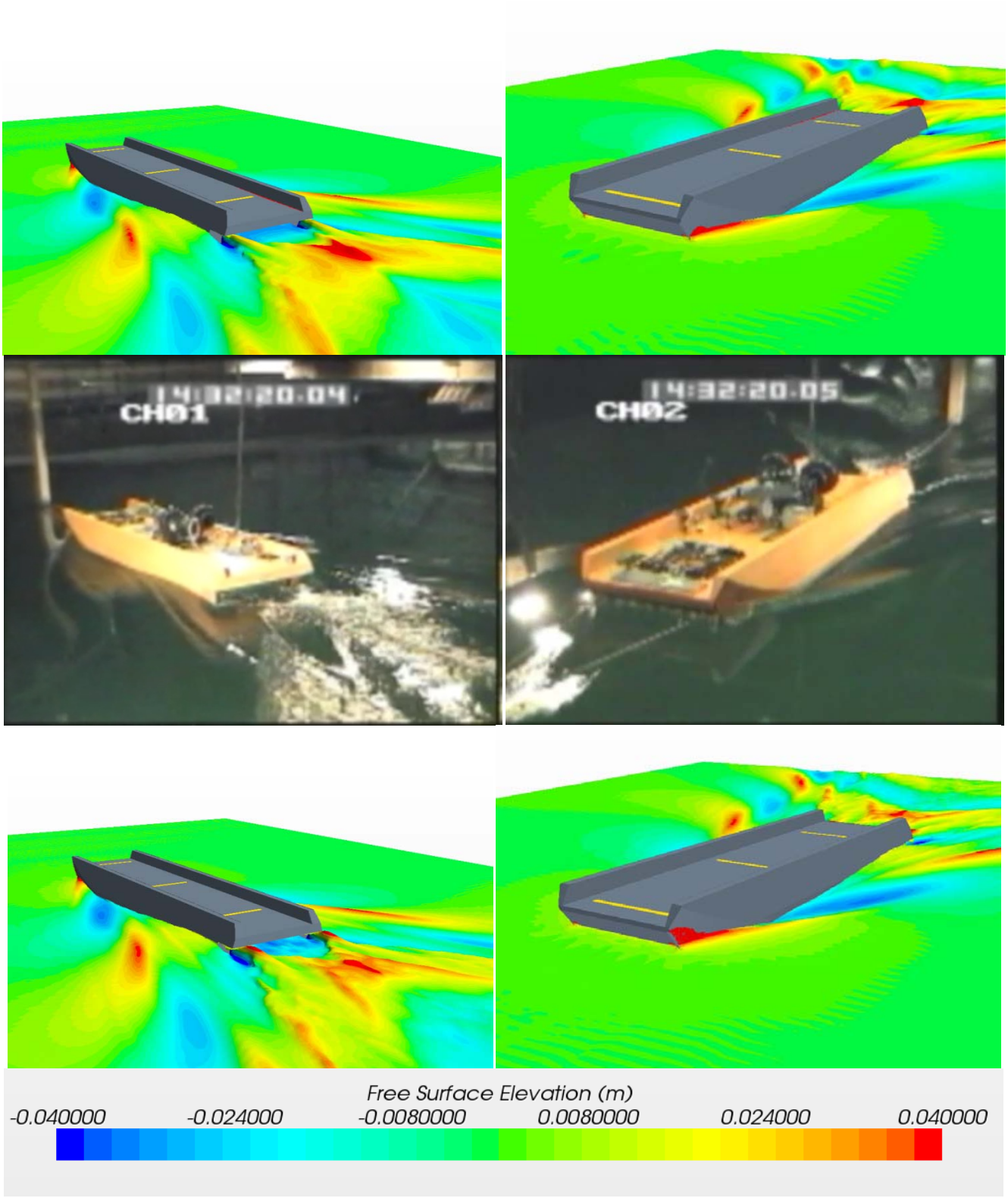

Figure 47: Free surface, Fn 0.4, Top: viscous simulation, Bottom: inviscid simulation

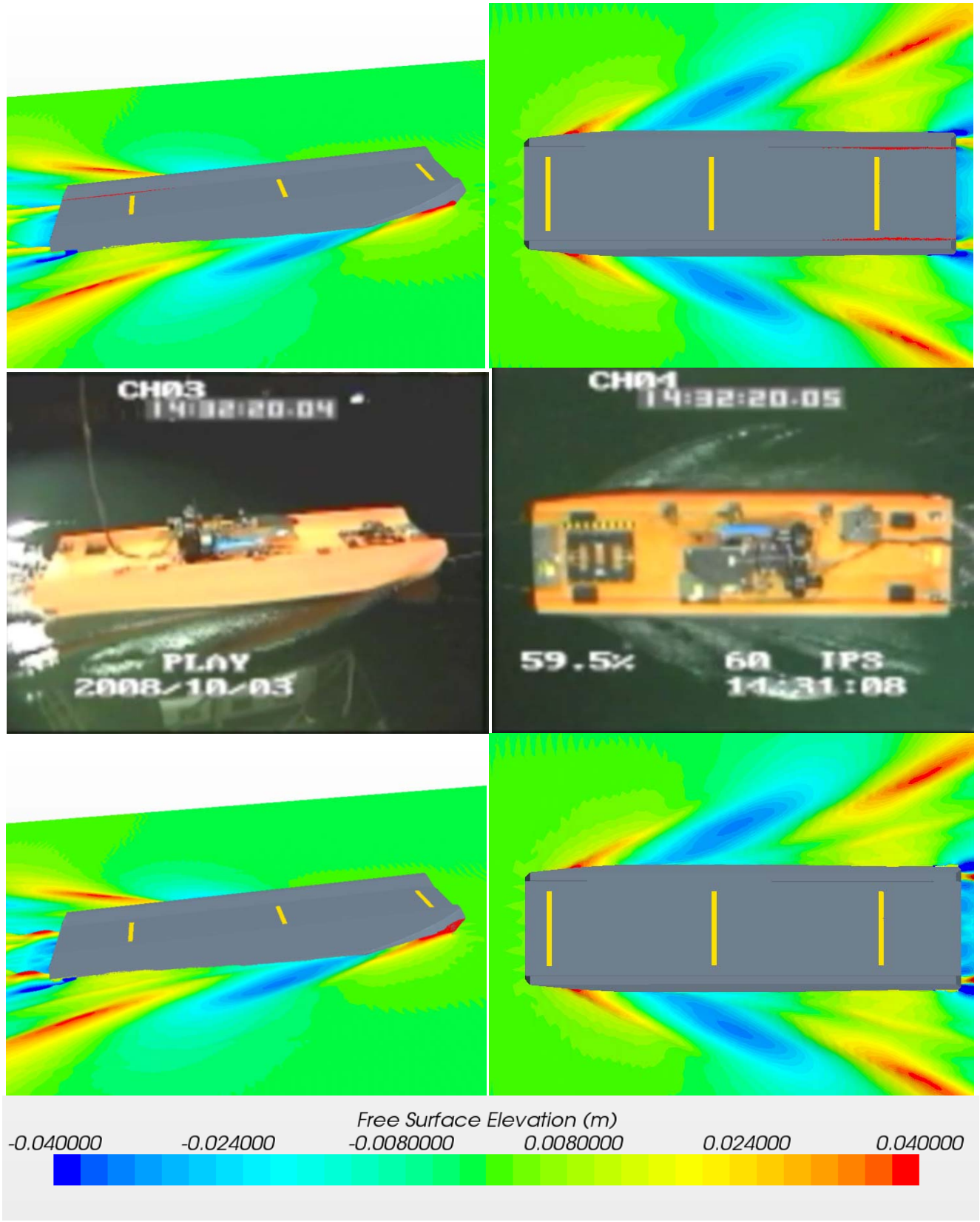

Figure 48: Free surface, Fn 0.4, Top: viscous simulation, Bottom: inviscid simulation

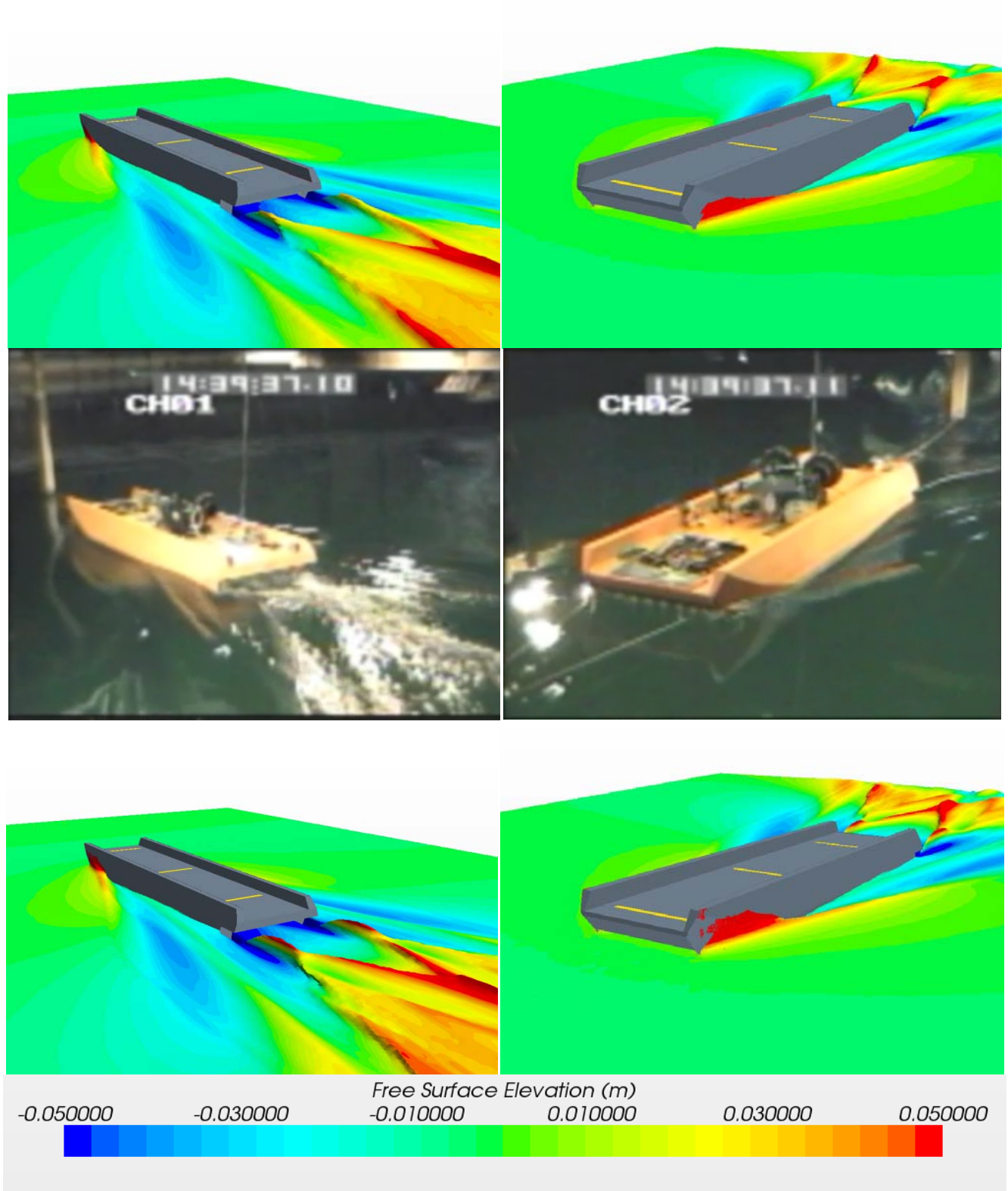

Figure 49: Free surface, Fn 0.6, Top: viscous simulation, Bottom: inviscid simulation

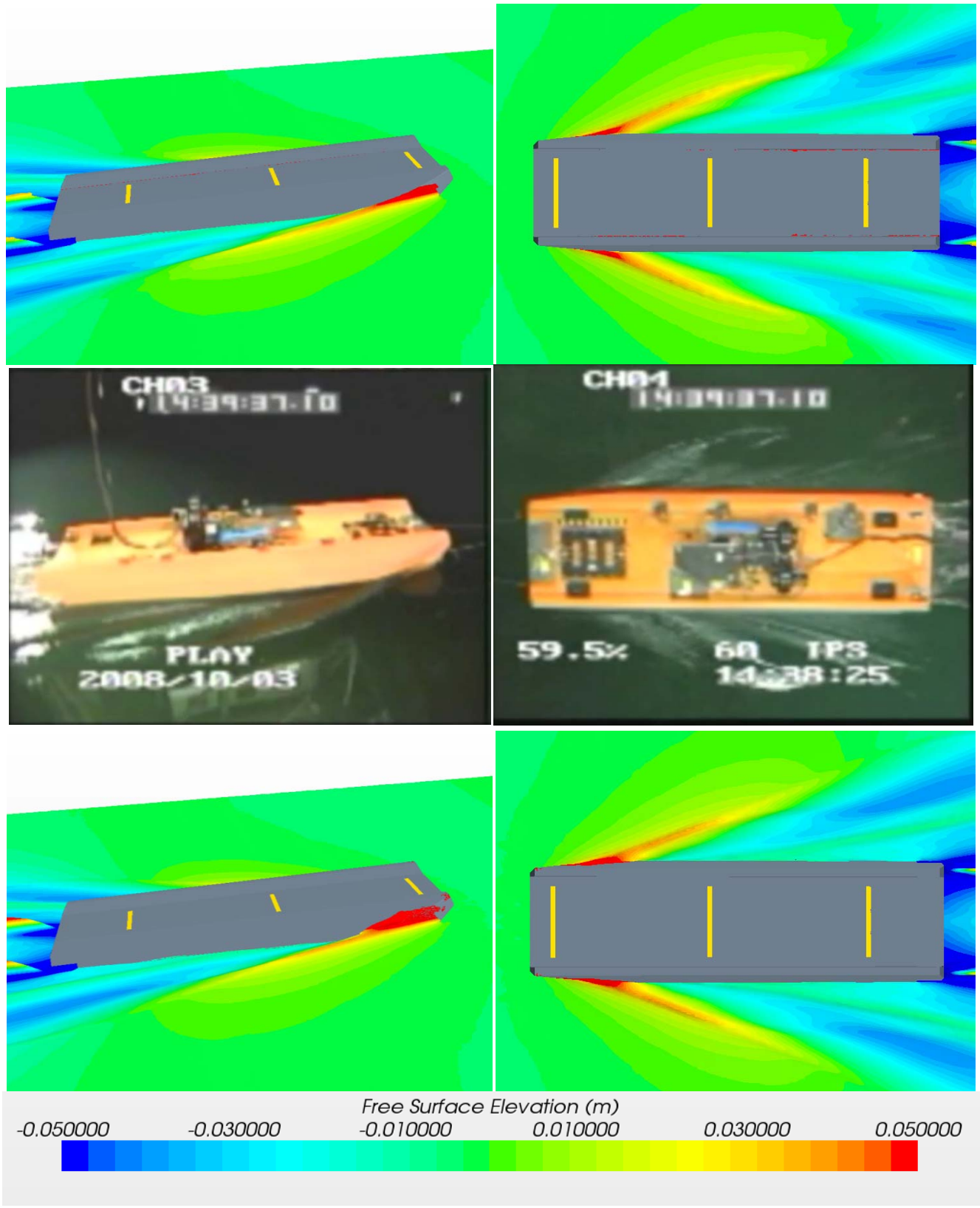

Figure 50: Free surface, Fn 0.6, Top: viscous simulation, Bottom: inviscid simulation

6. Conclusions and Discussion

It is clear that accurately simulating the motions, forces, and free surface interactions of a surface effect ship with a pressurized air cushion using CFD is a daunting task that involves several components. While the simulations presented show the promise of current commercial CFD modelling capabilities, much more must be done to improve the accuracy of the simulations. It is believed that the largest source of error is due to the rigid seal approximations. To accurately model the forces on an SES with flexible seals, the simulation's seals must also be dynamic. Shortening the rigid seals to above the natural waterline prevents them from plowing through the water, however it may under estimate the seal drag and it leaves a large gap for air leakage. Lengthening the seals to below the waterline does not allow any air leakage and causes a gross over estimation of the seal drag. As the long, rigid seals plow through the water they cause an exaggeration of the heave, pitch, and drag forces on the craft, especially in waves. If a dynamic seal model can be implemented that will accurately estimate the air leakage through the seals, an updated fan model can be implemented. The fan characteristics can be input into the momentum source and the fan RPM and flow rates can be matched to model test data which would help better estimate the pressure fluctuations in waves.The work presented is part of an ongoing study at Virginia Tech to incorporate dynamic and flexible seals into the simulations to more accurately simulate SES using CFD.

For the inviscid simulations,another source of error is due to the lack of viscous effects and forces in the simulations. When comparing inviscid simulations to simulations with viscosity,wave amplitudes were smaller with viscosity turned on due to viscous damping, however both types of simulations produced similar wakes that qualitatively match the model test videos.

While using a viscous solver and a prism layer mesh reveals any turbulent structures and allow the calculation of shear drag on the hull, the difference between the free surface of the inviscid and viscous solutions was small. The shear drag on the hull was shown to account for almost 25% of the total drag for each of the model test simulations and even more at higher speeds. This proves to be a large source of error when viscosity is neglected. A downfall to simulating viscosity is a large increase in simulation run time, as more complex equations must be solved at each timestep. Also an increased number of cells is typically needed for viscous simulation for the required prism layer. Adding the shear drag calculated using the ITTC-1957 friction coefficient line to the total drag from the inviscid simulations gives the total drag from the viscous simulations within 6% difference, providing an accurate and quick estimation of the viscous drag forces.Other turbulence models such as K-Omega and K-Epsilon should be investigated.

The capabilities of using three degrees of freedom, external forces, and waves are demonstrated in this work. The waves work can be expanded into simulations of irregular waves and waves from different headings. Enabling more degrees of freedom can allow for work to be done towards making response amplitude operators for an SES. Further expanding the work with external forces can lead to calculating dynamic powering requirements and modelling the SES's propulsion.

Separating the drag into components offers further insight to the forces at work in the simulation. Monitoring the drag from each of the seals and the hull separately helps reveal how much of an effect the rigid seal approximation is really having on the solution. While the effect of the wavemaking drag due to the air cushion is overshadowed by other drag sources, it is revealed when the drag is broken into components. Further breaking down the hull pressure drag into the wavemaking drag from the side hulls and the wavemaking drag due to the air cushion may prove useful.

After reviewing the free surface elevation contours, the complexity of the waves internal to the hull and air cushion at lower Froude is apparent. Both the amplitude and wavelength of these waves increase with speed. These waves are three dimensional and have unique interactions with the side hulls and seals at different Froude numbers. This work has proven that commercial CFD can be a useful tool in the calculation and visualization of these waves.

References

Bishop, R. C., Silver, A. L., Tahmasian, D., Lee, S. S., .Park, J. T, Snyder, L. A., and Kim, J. 2010. "T-Craft Seakeeping Model Test Data Report-Update" NSWCCD-50-TR–2010-062, Hydro-mechanics Department Report.

Cooper, K. "Sea Base Enabler Innovative Naval Prototype Transformable Craft (T-Craft), SD-5 Panel Brief" 2009 Office of Naval Research.

Doctors, L. and McKesson, C. "The Resistance Components of a Surface-Effect Ship", The Twenty-Sixth Symposium on Naval Hydrodynamics. Rome, Italy. September 2006.

Faltinsen, Odd M. *Hydrodynamics of High-Speed Marine Vehicles,* 2005. Cambridge University Press, New York, NY, USA

Lin, W, Zhang, S, and Weems, K. "Numerical Simulations of Surface Effect Ship in Waves", Proceedings 2010 Grand Challenges in Simulation and Modeling, July, 12-14, Ottawa, ON, Canada

Muzaferija,S. and Perić, M. "Computation of free-surface flows using interface-tracking and interface-capturing methods", Chap. 2 in O. Mahrenholtz and M. Markiewicz (eds.), *Nonlinear Water Wave Interaction,* Computational Mechanics Publications, Southampton, 1998.

"ONR awards $10.1 million T-Craft design contract". Marine Log. May 5, 2008. http://www.marinelog.com/DOCS/NEWSMMVII/2008may00053.html

Scullen, D. and Tuck, E. "Sea Wave Pattern Evaluation-Pressure Distributions: Mathematical Formulation". Scullen and Tuck Pty Ltd, July 2001.

Silver, A.Personal communication.2010, Ft. Lauderdale.

Star-CCM+ ver. 5.04.006 User Guide, 2010 CD-adapco.

Tuck, E., Scullen, D. and Lazauskas L. "Wave Patterns and Minimum Wave Resistance for High-Speed Vessels", 24th Symposium on Naval Hydrodynamics. Fukuoka, Japan. July 2002.

Yun, L. and Bliault, A. *Theory and Design of Air Cushion Craft*, 2000, L. Yun and A. Bliault, Bath Press, GreatBritain